Critical fluctuations and entanglement in the nondegenerate parametric oscillator

K. Dechoum,[1,2] P. D. Drummond,[1] S. Chaturvedi,[3] and M. D. Reid[1]
[1]*Australian Centre for Quantum-Atom Optics, The University of Queensland, St Lucia 4067, Queensland, Australia*
[2]*Instituto de Física da Universidade Federal Fluminense, Boa Viagem 24210-340, Niterói, Rio de Janeiro, Brazil*
[3]*School of Physics, University of Hyderabad, Hyderabad 500046, India*
(Received 21 October 2003; revised manuscript received 8 April 2004; published 5 November 2004)

We present a fully quantum mechanical treatment of the nondegenerate optical parametric oscillator both below and near threshold. This is a nonequilibrium quantum system with a critical point phase transition, that is also known to exhibit strong yet easily observed squeezing and quantum entanglement. Our treatment makes use of the positive *P* representation and goes beyond the usual linearized theory. We compare our analytical results with numerical simulations and find excellent agreement. We also carry out a detailed comparison of our results with those obtained from stochastic electrodynamics, a theory obtained by truncating the equation of motion for the Wigner function, with a view to locating regions of agreement and disagreement between the two. We calculate commonly used measures of quantum behavior including entanglement, squeezing, and Einstein-Podolsky-Rosen (EPR) correlations as well as higher order tripartite correlations, and show how these are modified as the critical point is approached. These results are compared with those obtained using two degenerate parametric oscillators, and we find that in the near-critical region the nondegenerate oscillator has stronger EPR correlations. In general, the critical fluctuations represent an ultimate limit to the possible entanglement that can be achieved in a nondegenerate parametric oscillator.

DOI: 10.1103/PhysRevA.70.053807 PACS number(s): 42.65.Yj, 03.67.Mn

I. INTRODUCTION

Nonlinear optical devices such as optical parametric oscillators (OPO's) and optical parametric amplifiers [1] have been studied in the last 40 years to provide fundamental tests of quantum mechanics, as well as for their technological applications in areas such as frequency conversion, low noise optical measurement, squeezed light sources [2], and cryptography. Nondegenerate optical parametric oscillators, in particular, display intensity correlations [3] and very short correlation times between the conjugate beams [4]. The entangled nature of the photons in the down-converted light has been instrumental in providing experimental demonstrations [5–8] of the original Einstein-Podolsky-Rosen paradox and other nonclassical features of quantum mechanics. In this paper, we extend the linear theory of the nondegenerate OPO to include nonlinear effects characteristic of the onset of critical fluctuations near threshold, which is the physical feature that ultimately limits the maximum squeezing and entanglement available.

As a fundamental application of these results, we point out that in 1935 Einstein, Podolsky, and Rosen (EPR) [9] presented their famous argument which demonstrates that local realism is inconsistent with the completeness of quantum mechanics. Their argument concerned two spatially separated particles with perfectly correlated positions and momenta, as predicted by quantum mechanics. Related correlations for quadrature phase operators have been studied [10–12] and experimentally confirmed for the output fields of the nondegenerate parametric oscillator, both below [5,6] and above [13] threshold. The study of these correlations has so far been confined to regimes of operation where the quantum fluctuations are small, so that a linearized analysis is valid.

Closely linked with the phenomenon of EPR correlations is that of entanglement, a key feature enabling many potential applications in the field of quantum information. Criteria for proving entanglement using continuous variable (quadrature phase amplitude) measurements have been developed by Duan *et al.* and Simon [14]. Recent experiments [7,15,16] have measured such continuous variable entanglement but again the studies are limited to the regime of stable, linearizable quantum fluctuations. In this regime Gaussian statistics apply, and the criterion developed can be shown [14] to be both a necessary and sufficient condition for entanglement in this case.

It is known from earlier theoretical analyses [17,18] of the optical properties of nonlinear interferometers that, in the linearized or Gaussian regime, a local realistic theory based on the Wigner phase space representation gives the same results for the correlations between signal and idler light beams produced in nonlinear crystals [17,18]. While this is also true of many correlations in second harmonic generation [19], there are instances where significant differences exist between the predictions of the two theories [20]. Here we calculate the EPR and entanglement measures for non-Gaussian fields, in precisely the type of environment where non-Gaussian behavior is expected to occur experimentally—that is, by considering nonlinear corrections to the usual linearized approximations used to treat the OPO below threshold.

In two recent papers [21,22] we have carried out a fully quantum mechanical analysis of nonlinear effects and critical fluctuations in a degenerate OPO using the positive *P* representation, and have investigated the squeezing spectra and triple correlations in this system both analytically as well as numerically. In particular, we have shown that, in this case, while the full quantum theory and the semiclassical theory disagree strongly far below threshold, there is a surprising agreement between the two close to the threshold where

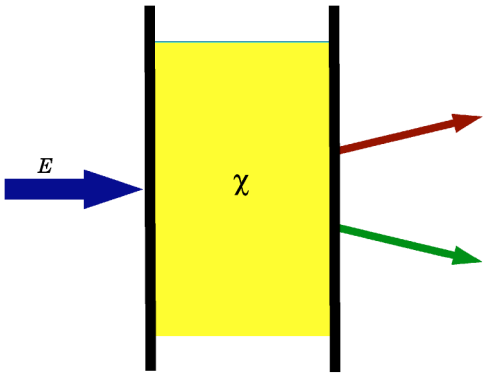

FIG. 1. Schematic diagram of a driven nondegenerate parametric oscillator.

quantum fluctuations are quite intense, characteristic of a mixed state of light in this limit.

The aim of the present work is to present a similar analysis for the case of a nondegenerate optical parametric oscillator. Both the quantum mechanical and semiclassical analyses are carried out in parallel and are compared with exact numerical simulations. Special attention is paid to the behavior of this system close to the critical point to ascertain the limits of entanglement, EPR correlations, and squeezing in this regime. We find that entanglement is optimized just below the critical point for output mode entanglement and squeezing, while the optimum internal squeezing and entanglement is achieved just above threshold. The results are compared with a configuration in which two degenerate parametric oscillators are combined to obtain correlated outputs. We find that, while these have similar behavior in the linearized region well below threshold, the single nondegenerate oscillator has greater optimal correlations near threshold, given the same total pump power.

II. HAMILTONIAN AND STOCHASTIC EQUATIONS

We consider here the standard model for three modes coupled by a nonlinear crystal inside a Fabry-Pérot interferometer with allowance made for coherent pumping and damping due to cavity losses. The general development of this type of open system theory is well described in the literature. This model implies certain restrictions on mode spacing for its validity, since we assume only these three modes are excited. A schematic diagram is shown in Fig. 1.

A. Hamiltonian

The Heisenberg-picture Hamiltonian that describes this open system is given by [12,23,24]

$$\hat{H} = \sum_{i=0}^{2} \hbar\omega_i \hat{a}_i^\dagger \hat{a}_i + i\hbar\chi(\hat{a}_1^\dagger \hat{a}_2^\dagger \hat{a}_0 - \hat{a}_1 \hat{a}_2 \hat{a}_0^\dagger) + i\hbar(\mathcal{E}e^{-i\omega_0 t}\hat{a}_0^\dagger - \mathcal{E}e^{i\omega_0 t}\hat{a}_0) + \sum_{i=0}^{2} (\hat{a}_i \hat{\Gamma}_i^\dagger + \hat{a}_i^\dagger \hat{\Gamma}_i). \tag{2.1}$$

Here $\mathcal{E}$ represents the external input field at a frequency ω_0, with $\hat{a}_0$, $\hat{a}_1$, and $\hat{a}_2$ representing the pump, signal, and idler intracavity modes at frequencies ω_0, ω_1, and ω_2, respectively, where $\omega_0 = \omega_1 + \omega_2$. The terms $\hat{\Gamma}_i$ represent reservoir operators and χ denotes the nonlinear coupling constant due to the second order polarizability of the nonlinear crystal.

This is a driven system far from thermal equilibrium, so it is not appropriate to assume a canonical ensemble. Instead, the density matrix must be calculated as the solution of a master equation in the Schrödinger picture. For simplicity, we transform to a rotating frame in which the free-field time evolution is removed. The master equation for the reduced density operator, obtained after the elimination of the reservoirs using standard techniques [25], is given by

$$\frac{\partial \hat{\rho}}{\partial t} = \chi[\hat{a}_1^\dagger \hat{a}_2^\dagger \hat{a}_0 - \hat{a}_1 \hat{a}_2 \hat{a}_0^\dagger, \hat{\rho}] + \mathcal{E}[\hat{a}_0^\dagger - \hat{a}_0, \hat{\rho}] + \sum_{i=0}^{2} \gamma_i (2\hat{a}_i \hat{\rho} \hat{a}_i^\dagger - \hat{a}_i^\dagger \hat{a}_i \hat{\rho} - \hat{\rho} \hat{a}_i^\dagger \hat{a}_i), \tag{2.2}$$

where γ_i are the damping rates for the mode amplitudes. For simplicity, we assume that $\gamma_1 = \gamma_2 = \gamma$ throughout this paper.

To handle master equations such as this it proves convenient to transform them into *c*-number Fokker-Planck equations or equivalently into stochastic equations using operator representation theory. Here, as in our earlier work, we use the positive *P* representation for this purpose, and we also compare these results with the approximate semiclassical truncation of the Wigner representation.

B. The positive *P* representation

Using the positive *P* representation [26], we can include correlations and fluctuations by expanding the density matrix describing the system in an off-diagonal coherent state basis as

$$\hat{\rho} = \int \frac{|\boldsymbol{\alpha}\rangle\langle(\boldsymbol{\alpha}^+)^*|}{\langle(\boldsymbol{\alpha}^+)^*|\boldsymbol{\alpha}\rangle} P_+(\boldsymbol{\alpha}, \boldsymbol{\alpha}^+) d^6\boldsymbol{\alpha} d^6\boldsymbol{\alpha}^+ \tag{2.3}$$

where $\boldsymbol{\alpha} \equiv (\alpha_0, \alpha_1, \alpha_2)$ and $\boldsymbol{\alpha}^+ \equiv (\alpha_0^+, \alpha_1^+, \alpha_2^+)$ are two independent triplets of complex variables. The function $P(\boldsymbol{\alpha}, \boldsymbol{\alpha}^+)$ is a positive phase space distribution and, by virtue of Eq. (2.3), satisfies the following Fokker-Planck equation [12], assuming that boundary terms vanish on partial integration:

$$\frac{\partial P_+}{\partial t} = \left\{ \frac{\partial}{\partial \alpha_0}[\gamma_0\alpha_0 + \chi\alpha_1\alpha_2 - \mathcal{E}] + \frac{\partial}{\partial \alpha_0^+}[\gamma_0\alpha_0^+ + \chi\alpha_1^+\alpha_2^+ - \mathcal{E}] + \frac{\partial}{\partial \alpha_1}[\gamma_1\alpha_1 - \chi\alpha_0\alpha_2^+] + \frac{\partial}{\partial \alpha_1^+}[\gamma_1\alpha_1^+ - \chi\alpha_0^+\alpha_2] + \frac{\partial}{\partial \alpha_2}[\gamma_2\alpha_2 - \chi\alpha_0\alpha_1^+] + \frac{\partial}{\partial \alpha_2^+}[\gamma_2\alpha_2^+ - \chi\alpha_0^+\alpha_1] + \frac{\partial^2}{\partial \alpha_1 \partial \alpha_2}(\chi\alpha_0) + \frac{\partial^2}{\partial \alpha_1^+ \partial \alpha_2^+}(\chi\alpha_0^+) \right\} P_+(\alpha, \alpha^+, t). \tag{2.4}$$

This can equivalently be written as the following set of Itô stochastic equations [28]:

$$d\alpha_0 = (\mathcal{E} - \gamma_0\alpha_0 - \chi\alpha_1\alpha_2)dt,$$

$$d\alpha_0^+ = (\mathcal{E}^* - \gamma_0\alpha_0^+ - \chi\alpha_1^+\alpha_2^+)dt,$$

$$d\alpha_1 = (-\gamma_1\alpha_1 + \chi\alpha_2^+\alpha_0)dt + (\chi\alpha_0)^{1/2}dW_1,$$

$$d\alpha_1^+ = (-\gamma_1\alpha_1^+ + \chi\alpha_2\alpha_0^+)dt + (\chi\alpha_0^+)^{1/2}dW_1^+,$$

$$d\alpha_2 = (-\gamma_2\alpha_2 + \chi\alpha_1^+\alpha_0)dt + (\chi\alpha_0)^{1/2}dW_2,$$

$$d\alpha_2^+ = (-\gamma_2\alpha_2^+ + \chi\alpha_1\alpha_0^+)dt + (\chi\alpha_0^+)^{1/2}dW_2^+, \qquad (2.5)$$

where

$$\langle dW_1\rangle = \langle dW_2\rangle = 0,$$

$$\langle dW_1 dW_2\rangle = \langle dW_1^+ dW_2^+\rangle = dt, \qquad (2.6)$$

with all other noise correlations vanishing. These equations imply that $\langle\alpha_i\alpha_i^+\rangle = \langle\hat{n}_i\rangle = 0$ when there is no driving field, as physically expected for a vacuum state in a normally ordered representation.

Numerical simulations of these stochastic trajectories confirm the assumption of asymptotically vanishing boundary terms for the parameters we use, as the trajectories are strongly bounded to a compact domain. This is similar to earlier studies, where boundary terms were found to be exponentially suppressed for large damping [27]—i.e., $\gamma_i \gg \chi$, which corresponds to typical experimental conditions for realistic OPO's in current use. At smaller damping rates, it would become important to include stochastic gauge terms [30] in the equations to eliminate boundary terms, but this was not found to be necessary in these calculations. In other words, while boundary terms are potentially present, the resulting errors are expected to be of order $e^{-\gamma/\chi}$ or smaller, which is completely negligible in typical quantum optical systems where $\gamma/\chi \gg 1$.

C. The semiclassical theory

We can also transcribe the master equation as a *c*-number phase space evolution equation using the Wigner representation

$$P_W(\boldsymbol{\alpha},\boldsymbol{\alpha}^*) = \frac{1}{\pi^2}\int_{-\infty}^{\infty} d^6\mathbf{z}\,\chi_W(\mathbf{z},\mathbf{z}^*)e^{-i\mathbf{z}^*\cdot\boldsymbol{\alpha}^*}e^{-i\mathbf{z}\cdot\boldsymbol{\alpha}}, \quad (2.7)$$

where $\chi_W(\mathbf{z},\mathbf{z}^*)$, the characteristic function for the Wigner representation, is given by

$$\chi_W(\mathbf{z},\mathbf{z}^*) = \mathrm{Tr}(\rho e^{i\mathbf{z}^*\cdot\hat{\mathbf{a}}^\dagger + i\mathbf{z}\cdot\hat{\mathbf{a}}}). \qquad (2.8)$$

This transcription is particularly useful for semiclassical treatments.

The equation for the Wigner function for the nondegenerate parametric amplifier that corresponds to the master equation (2.2) turns out to be

$$\frac{\partial P_W}{\partial t} = \Bigg\{ \frac{\partial}{\partial\alpha_0}(\gamma_0\alpha_0 + \chi\alpha_1\alpha_2 - \mathcal{E}) + \frac{\partial}{\partial\alpha_0^*}(\gamma_0\alpha_0^* + \chi\alpha_1^*\alpha_2^* - \mathcal{E}) + \frac{\partial}{\partial\alpha_1}(\gamma_1\alpha_1 - \chi\alpha_2^*\alpha_0) + \frac{\partial}{\partial\alpha_1^*}(\gamma_1\alpha_1^* - \chi\alpha_2\alpha_0^*) + \frac{\partial}{\partial\alpha_2}(\gamma_2\alpha_2 - \chi\alpha_1^*\alpha_0) + \frac{\partial}{\partial\alpha_2^*}(\gamma_2\alpha_2^* - \chi\alpha_1\alpha_0^*) + \gamma_0\frac{\partial^2}{\partial\alpha_0\partial\alpha_0^*} + \gamma_1\frac{\partial^2}{\partial\alpha_1\partial\alpha_1^*} + \gamma_2\frac{\partial^2}{\partial\alpha_2\partial\alpha_2^*} + \frac{\chi}{4}\left(\frac{\partial^3}{\partial\alpha_1\partial\alpha_2\partial\alpha_0^*} + \frac{\partial^3}{\partial\alpha_1^*\partial\alpha_2^*\partial\alpha_0}\right)\Bigg\} P_W. \qquad (2.9)$$

If we drop the third order derivative terms, in an approximation valid in the limit of large photon number, we can equate the resulting truncated Fokker-Planck equation describing the evolution of the Wigner function with a set of Itô stochastic equations which read as follows:

$$d\alpha_0 = (\mathcal{E} - \gamma_0\alpha_0 - \chi\alpha_1\alpha_2)dt + \sqrt{\gamma_0}dW_0,$$

$$d\alpha_0^* = (\mathcal{E}^* - \gamma_0\alpha_0^* - \chi\alpha_1^*\alpha_2^*)dt + \sqrt{\gamma_0}dW_0^*,$$

$$d\alpha_1 = (-\gamma_1\alpha_1 + \chi\alpha_2^*\alpha_0)dt + \sqrt{\gamma_1}dW_1,$$

$$d\alpha_1^* = (-\gamma_1\alpha_1^* + \chi\alpha_2\alpha_0^*)dt + \sqrt{\gamma_1}dW_1^*,$$

$$d\alpha_2 = (-\gamma_2\alpha_2 + \chi\alpha_1^*\alpha_0)dt + \sqrt{\gamma_2}dW_2,$$

$$d\alpha_2^* = (-\gamma_2\alpha_2^* + \chi\alpha_1\alpha_0^*)dt + \sqrt{\gamma_2}dW_2^*. \qquad (2.10)$$

The nonvanishing noise correlations are given by

$$\langle dW_i\rangle = 0,$$

$$\langle dW_i dW_i^*\rangle = dt,\ i = 0,1,2. \qquad (2.11)$$

If we compare the two sets of Itô stochastic equations, namely, (2.5) and (2.10), we notice that the main difference between the two is in the structure of the noise terms. While the noise terms in the positive *P* equations (2.5) depend on the pumping amplitude and the nonlinear coupling constant, those in the Wigner representation do not. In fact they correspond precisely to the noise terms that one adds, in the linear case, in compliance with the fluctuation-dissipation theorem.

In some sense, one can interpret the noise terms in the Wigner case as accounting for vacuum fluctuations. However, the truncated Wigner theory must be treated cautiously, since it ignores important third order correlations which are not always negligible. These equations imply that $\langle\alpha_i\alpha_i^+\rangle = \langle\hat{n}_i\rangle = 1/2$ when there is no driving and no coupling, as expected for a vacuum state in a symmetrically ordered representation. However, a vacuum state is *not* obtained semiclassically if there is any coupling χ, even with a vacuum input, which is an unphysical feature. The full Wigner theory has no such limitations: but it is no longer positive definite and therefore has no equivalent stochastic formulation.

D. Comparison of methods

In both representations, the classical approximation, where all fluctuations are neglected, is equivalent to simply assuming that all operator mean values factorize. This gives us the classical nonlinear-optical equations for $\alpha_i = \langle \hat{a}_i \rangle$ in the form

$$\frac{\partial \alpha_0}{\partial t} = \mathcal{E} - \gamma_0 \alpha_0 - \chi \alpha_1 \alpha_2,$$

$$\frac{\partial \alpha_i}{\partial t} = -\gamma \alpha_i + \chi \alpha_{3-i}^{*} \alpha_0. \tag{2.12}$$

For small driving fields, the stable classical below-threshold solutions are $\alpha_0 = \mathcal{E}/\gamma_0$ and $\alpha_1 = \alpha_2 = 0$. There is a classical threshold or critical point at $\mathcal{E} = \mathcal{E}_c = \gamma\gamma_0/\chi$. Above this threshold, the driving field is clamped at $\alpha_c = \gamma/\chi$, with an intracavity photon number of $N_c = \gamma^2/\chi^2$, while the signal and idler intensities increase linearly with the input field $\mathcal{E}$. The critical input photon flux, assuming no other losses except through the input/output coupling, is given by

$$I_c = \frac{|\mathcal{E}_c|^2}{2\gamma_0} = \frac{N_c \gamma_0}{2}. \tag{2.13}$$

The Wigner truncation approximation does include quantum fluctuation effects, but ignores higher order terms in an expansion in $1/N_c$, which are important when calculating the corrections to the leading order linear fluctuations.

The positive P equations provide a more systematic route to including quantum fluctuations, since the neglect of boundary terms is well justified in these calculations as long as $\gamma/\chi = \sqrt{N_c} \gg 1$. If necessary, the technique can be checked with the more precise stochastic gauge approach [30]. No evidence was found that boundary terms were significant here, even for the relatively small values of $N_c \simeq 10^3$ used in the numerics. We will show that the truncated Wigner method gives rise to clearly unphysical predictions at low driving field, which does not occur with the positive P equations, given the parameters used here. Accordingly, we mainly focus on the positive P phase space method in this paper.

As an alternative, one might imagine that a direct numerical calculation in a photon number basis would be useful, provided the maximum photon number was small. We note that in a three-mode system the Hilbert space dimension scales as $n_{\max}^3$, while the density matrix has $n_{\max}^6$ components provided the boson number is bounded by $n_{\max}$. In practice, one finds that typical experiments have $n_{\max} \simeq N_c \simeq 10^3 - 10^9$. This implies that neither the full density matrix nor even the reduced wave function in a stochastic wave-function calculation [29] can in general be calculated directly with current computers, for practical reasons of memory and computational time. Direct number state methods are also not convenient for analytical approximations.

Other techniques involve Feynman (or related) diagrammatic techniques, using a hierarchy of correlation functions [31]. These methods give useful results below threshold, and have similarities to perturbation theory using stochastic methods, which we discuss later. The drawbacks are that these diagrammatic methods appear less systematic than phase space methods, since certain classes of diagrams are discarded, and the results usually diverge at the critical point.

III. OBSERVABLE MOMENTS AND EPR SPECTRA

In order to understand what types of calculation to carry out for this system, it is important to identify operational measurements, and relate these to operators and their correlations.

The positive P stochastic method directly reproduces the normally ordered correlations and moments, while the Wigner representation reproduces the symmetrically ordered moments. Of course, commutation relations can always be used to transform one type of ordering into the other. Further, we also have to distinguish between the internal and external operator moments, since measurements are normally performed on output fields that are external to the cavity. The necessary formalism for treating external field spectra was introduced and developed by Yurke [32] and by Gardiner and Collett [33].

As we shall see, there is a direct relationship between the output field spectra of a nondegenerate OPO and observable criteria for EPR correlations and entanglement.

A. Internal moments

The squeezing in terms of the intracavity quadrature covariances corresponds to an instantaneous measurement of the field moments. A general quadrature covariance is defined as

$$S_{ij}^{\theta} = \langle : \hat{X}_i^{\theta}(t) \hat{X}_j^{\theta}(t) : \rangle, \tag{3.1}$$

where a measurement of $S_{jj}^{\theta} < 0$ indicates intracavity squeezing in mode j, and we define

$$\hat{X}_j^{\theta} = e^{-i\theta} \hat{a}_j(t) + e^{i\theta} \hat{a}_j^{\dagger}(t) \tag{3.2}$$

to denote internal quadrature operators. Similarly, complex quadratures [35] are defined as

$$\hat{X}^{\theta} = e^{-i\theta} \hat{a}_1(t) + e^{i\theta} \hat{a}_2^{\dagger}(t) = \frac{1}{2}[\hat{X}_1^{\theta} + \hat{X}_2^{\theta} + i(\hat{X}_1^{\theta+\pi/2} - X_2^{\theta+\pi/2})], \tag{3.3}$$

with a normally ordered intracavity variance of

$$S^{\theta} = \langle : \hat{X}^{\theta}(t) \hat{X}^{\dagger\theta}(t) : \rangle = \frac{1}{4} \langle : (\hat{X}_1^{\theta} + \hat{X}_2^{\theta})^2 : \rangle + \frac{1}{4} \langle : (\hat{X}_1^{\theta+\pi/2} - \hat{X}_2^{\theta+\pi/2})^2 : \rangle. \tag{3.4}$$

If such measurements were possible, they would include contributions from all frequencies. However, it is more typical that one has access to spectrally resolved quadrature measurements of the output fields, and these are generally more useful as measures of entanglement and squeezing.

B. External spectra

The external field measurements are obtained from the input-output relations [32,33]

$$\hat{\Phi}_j^{out}(t) = \sqrt{2\gamma_j^{out}}\hat{a}_j(t) - \hat{\Phi}_j^{in}(t), \tag{3.5}$$

where $\hat{\Phi}_j^{in}(t)$ and $\hat{\Phi}_j^{out}(t)$ are the input and output photon fields, respectively, evaluated at the output-coupling mirror, and $\hat{a}_j(t)$ is the intracavity photon field. The most efficient transport of squeezing is obtained if we assume that all the signal losses occur through the output coupler, so that $\gamma_1 = \gamma_1^{out}$. We will assume this to be the case for simplicity, though the necessary corrections [12] for imperfect interferometers simply involve the ratio γ_j^{out}/γ_j.

The measured output spectral covariance V_{ij}^{θ} of a general quadrature

$$\hat{X}_j^{\theta\ out} = e^{-i\theta}\hat{\Phi}_j^{out}(t) + e^{i\theta}\hat{\Phi}_j^{\dagger out}(t) \tag{3.6}$$

can be written as

$$V_{ij}^{\theta}(\omega) = \langle \Delta\hat{X}_i^{\theta\ out}(\omega)\Delta\hat{X}_j^{\theta\ out}(\omega')\rangle, \tag{3.7}$$

where the fluctuations $\Delta\hat{X}_j^{\theta\ out}$ are defined as $\Delta\hat{X}_j^{\theta\ out} = \hat{X}_j^{\theta\ out} - \langle\hat{X}_j^{\theta\ out}\rangle$, θ is the phase angle related to a phase-sensitive local oscillator measurement, and the frequency argument denotes a Fourier transform:

$$\hat{X}_j^{\theta\ out}(\omega) = \frac{1}{T}\int_{-T/2}^{T/2} dt e^{i\omega t}\hat{X}_j^{\theta\ out}(t). \tag{3.8}$$

We also introduce complex quadratures and their Fourier transforms, which are useful for computational purposes:

$$\hat{X}^{\theta\ out} = e^{-i\theta}\hat{\Phi}_1^{out}(t) + e^{i\theta}\hat{\Phi}_2^{\dagger out}(t),$$

$$\hat{X}^{\dagger\theta\ out} = e^{-i\theta}\hat{\Phi}_2^{out}(t) + e^{i\theta}\hat{\Phi}_1^{\dagger out}(t),$$

$$\hat{X}^{\theta\ out}(\omega) = \frac{1}{T}\int_{-T/2}^{T/2} dt e^{-i\omega t}\hat{X}^{\theta\ out}(t),$$

$$\hat{X}^{\dagger\theta\ out}(\omega) = \frac{1}{T}\int_{-T/2}^{T/2} dt e^{i\omega t}\hat{X}^{\dagger\theta\ out}(t). \tag{3.9}$$

The spectral quadrature operators $\hat{X}_i^{\theta\ out}(\omega)$ are *not* formally Hermitian except at $\omega=0$.

C. Observable quadratures

In practice, one is mostly interested in external spectral measurements taken over a long but finite interval, after a steady state is achieved. For output measurements averaged over a long time T, it is the low frequency part of the spectrum that is the relevant quantity, as it usually determines the maximum squeezing or entanglement possible. For simplicity, we will focus on the $\omega=0$ case, where we can define *observable* frequency-domain quadrature operators as

$$\hat{X}_i^{out} = \hat{X}_i^{0\ out}(0),$$

$$\hat{Y}_i^{out} = \hat{X}_i^{\pi/2\ out}(0), \tag{3.10}$$

which have the usual commutators of $[\hat{X}_i^{out}, \hat{Y}_j^{out}] = 2i\delta_{ij}$.

Since the mean values are zero for down-conversion below threshold, the zero-frequency complex quadrature spectrum for the combined quadrature is

$$V^{\theta}(0) = \langle \hat{X}^{\theta\ out}(0)\hat{X}^{\dagger\theta\ out}(0)\rangle. \tag{3.11}$$

In particular, the most important spectra are the unsqueezed and squeezed spectra defined by

$$V^0(0) = \frac{1}{4}\langle[\hat{X}_1^{out} + \hat{X}_2^{out}]^2 + [\hat{Y}_1^{out} - \hat{Y}_2^{out}]^2\rangle,$$

$$V^{\pi/2}(0) = \frac{1}{4}\langle[\hat{Y}_1^{out} + \hat{Y}_2^{out}]^2 + [\hat{X}_1^{out} - \hat{X}_2^{out}]^2\rangle. \tag{3.12}$$

In other words, the complex quadrature spectra simply correspond to simultaneous sum and difference measurements on the two observed output quadratures for the signal and idler, with the precise quadratures observed adjustable via the local oscillator phase angle θ.

The properties of external quadratures for $\omega \neq 0$ are experimentally important since technical noise normally prohibits direct quadrature measurements at $\omega=0$. Nevertheless, even at $\omega \neq 0$ the quadratures are decomposable [12] into pairs of mutually commuting Hermitian operators with similar properties to the intracavity quadrature operators, by using discrete sine and cosine transforms. These results therefore hold at nonzero frequencies.

The correlations are closely related to those proposed by EPR. We will give more details in the next section, explaining the relationship of this type of measurement with the EPR paradox and entanglement.

D. Stochastic mappings of operator moments

We now wish to relate these observed operator correlations with the stochastic correlations that are used to calculate them via the *c*-number equivalences.

1. P representation

In the *P* representation normally ordered operator averages directly relate to stochastic moments of the positive *P* function:

$$\langle :\hat{X}_j^{\theta}(t)\hat{X}_j^{\theta}(t):\rangle = \langle X_j^{\theta}(t)X_j^{\theta}(t)\rangle_P, \tag{3.13}$$

where the internal stochastic variables corresponding to the quadratures are denoted by

$$X_j^{\theta} = (\alpha_j e^{-i\theta} + \alpha_j^{+} e^{i\theta}). \tag{3.14}$$

The positive *P* spectral correlations correspond to the normally ordered, time-ordered operator correlations of the measured fields. This leads to the following well-known result for the general squeezing spectrum, as measured in an external homodyne detection scheme:

$$V_{ij}^{\theta}(\omega)\delta(\omega+\omega') = \delta_{ij} + 2\sqrt{\gamma_i^{out}\gamma_j^{out}}\langle \Delta\tilde{X}_i^{\theta}(\omega)\Delta\tilde{X}_j^{\theta}(\omega')\rangle_P. \tag{3.15}$$

This calculation involves only the internal stochastic quadrature spectral variables, defined as

$$\Delta\tilde{X}_j^{\theta}(\omega) = \int \frac{dt}{\sqrt{2\pi}} e^{i\omega t}(X_j^{\theta}(t) - \langle X_j^{\theta}(t)\rangle_P). \tag{3.16}$$

Note that reflected vacuum input field terms from Eq. (3.5) do not contribute directly to this spectrum, as they have a vanishing normally ordered spectrum and are not correlated with the coherent amplitudes in the positive *P* representation.

2. Wigner representation

In the Wigner representation, on the other hand, the moments and correlations with respect to the Wigner function are directly related to averages of symmetrically ordered operators. It becomes necessary to rewrite the normally ordered internal field averages in terms of symmetrically ordered averages using equal-time commutators. As a result the two spectral orderings are related by

$$\langle :\hat{X}_i^{\theta}(t)\hat{X}_j^{\theta}(t):\rangle = \langle X_i^{\theta}(t)X_j^{\theta}(t)\rangle_W - \delta_{ij}. \tag{3.17}$$

Similarly, for the normally ordered squeezing spectrum, as measured in an external homodyne detection scheme, one has

$$V_{ij}^{\theta}(\omega)\delta(\omega+\omega') = \langle \Delta\tilde{X}_i^{\theta\ out}(\omega)\Delta\tilde{X}_j^{\theta\ out}(\omega')\rangle_W. \tag{3.18}$$

Here we define Fourier transforms of fluctuations as previously, except with respect to stochastic output fields

$$X_j^{\theta\ out} = e^{-i\theta}\Phi_j^{out}(t) + e^{i\theta}\Phi_j^{\dagger out}(t), \tag{3.19}$$

where

$$\Phi_j^{out}(t) = \sqrt{2\gamma^{out}}\alpha_j - \Phi_j^{in}(t). \tag{3.20}$$

It is essential to include the vacuum field contributions from reflected input fields as in Eq. (3.5), as these are correlated with the internal Wigner amplitudes and hence contribute significantly to the spectrum. In fact, these input fields can be shown to correspond directly to the noise terms in the Wigner representation stochastic equations, leading to the identification

$$\frac{dW_j}{dt} = \sqrt{2}\Phi_j^{in}(t), \tag{3.21}$$

where $\Phi_j^{in}(t)$ is a *c*-number amplitude corresponding (in the Wigner representation) to the quantum vacuum input field, and $\langle \Phi_j^{in}(t)\Phi_j^{*in}(t')\rangle_W = \delta(t-t')/2$.

The fundamental property of the Wigner function is that the ensemble average of any polynomial of the random variables α and α^* weighted by the Wigner density exactly corresponds to the Hilbert-space expectation of the corresponding symmetrized product of the annihilation and creation operators. Therefore, the truncated theory with a positive Wigner function can be viewed as equivalent to a hidden variable theory, since one can obtain quadrature fluctuation predictions by following an essentially classical prescription; in which even the noise terms have a classical interpretation as corresponding a form of zero-point fluctuations. This description cannot be equivalent to quantum mechanics in general, but may provide results which, under some circumstances, turn out to be quite similar to the quantum mechanical results.

IV. EPR CORRELATIONS AND ENTANGLEMENT

A quantitative, experimentally testable criterion for the EPR paradox was proposed in 1989 [11]. It is important to understand the physical interpretation of this paradox. EPR originally assumed local realism, and claimed that an observation of perfectly correlated positions and momenta would imply the incompleteness of quantum mechanics. A modern interpretation is that one can merely deduce the *inconsistency* of local realism with quantum mechanical completeness, since local realism in Einstein's original sense is no longer widely accepted. This is a weaker paradox than the Bell inequality—which rules out all local realistic interpretations. However, the Bell inequality has not yet been violated, due to causality and/or measurement inefficiency issues (though weaker inequalities have been violated). The EPR paradox with quadrature variables has the advantage that the required degree of measurement efficiency is readily achievable with photodetectors, since it does not require single-photon counting.

A. 1989 EPR criterion: Violation of an inferred Heisenberg uncertainty principle

Consider two spatially separated subsystems at *A* and *B*. Observables $\hat{X}_1$ ("position") and $\hat{Y}_1$ ("momentum") are defined for subsystem *A*, where the two operators have a commutator of $[\hat{X}_1,\hat{Y}_1]=2i$, so that by Heisenberg's uncertainty principle $\Delta^2\hat{X}_1\Delta^2\hat{Y}_1 \geqslant 1$. Suppose that the two subsystems are partially correlated, as may occur in a real experiment, as opposed to the ideal correlations in the EPR gedanken experiment. One may still predict the result of measurement $\hat{X}_1$, based on the result of a causally separated measurement $\hat{X}_2$ performed at *B*. However, the prediction is imperfect, and has an associated inference error. Also, for a different choice of measurement $\hat{Y}_2$ at *B*, suppose that one may predict the result of measurement $\hat{Y}_1$ at *A*.

We define

$$\Delta_{inf}^2 X_1 = \int P(X_2)\Delta^2(X_1|X_2)dX_2,$$

$$\Delta_{inf}^2 Y_1 = \int P(Y_2)\Delta^2(Y_1|Y_2)dY_2. \tag{4.1}$$

Here X_2 labels all outcomes of the measurement $\hat{X}_2$ at *B*, and $\Delta^2(X_1|X_2)$ is the variance of the conditional distribution $P(X_1|X_2)$, where X_1 is the conditional result of the measurement $\hat{X}_1$ at *A*, given the measurement $\hat{X}_2$ at *B*. The probabil-

ity $P(X_2)$ is the probability for a result X_2 upon measurement of $\hat{X}_2$.

Next, we define an inference variance $\Delta^2_{inf}\hat{X}_1$ as the average variance of the conditional (inference) variances $\Delta(X_1|X_2)$ for the prediction (inference) of the result X_1 for $\hat{X}_1$ at A, conditional on a measurement $\hat{X}_2$ at B. We define $\Delta(Y_1|Y_2)$ similarly to represent the weighted variance associated with the prediction (inference) of the result $\hat{Y}_1$ at A, based on the result of the measurement at B.

The 1989 inferred Heisenberg uncertainty principle (HUP) criterion [11] to demonstrate EPR correlations is

$$\Delta_{inf}X_1\Delta_{inf}Y_1 < 1. \tag{4.2}$$

This EPR-style criterion (4.2) was not given in the original EPR paper, but has the useful property that it represents a quantitative inequality that can be experimentally satisfied, without having to construct an experimentally impossible state with perfect correlations, as in the original proposal. As an added advantage, the application of this inequality to electromagnetic quadrature variables allows the use of efficient photodetection techniques, which makes this a completely practical measure.

By contrast, the violation of a Bell inequality—while having stronger consequences—is more difficult to achieve, owing to poor efficiencies encountered in single-particle detectors and polarizers. For either type of experiment, a crucial element is the causal separation of detectors. Without this, arguments using causality provide no constraints or inequalities at all.

Linear estimate criterion

It is not always convenient to measure each conditional distribution $P(X_1|X_2)$ and $P(Y_1|Y_2)$ and its associated mean and variance. A simpler procedure [11] is to propose that upon a result X_2 for the measurement at B the predicted value for the result X_1 at A is given linearly by the estimate $X_{est}=cX_2+d$. The rms error in this estimate after optimizing for d is

$$\Delta^2_{inf,L}\hat{X}_1 = \langle \delta_0^2\rangle - \langle \delta_0\rangle^2, \tag{4.3}$$

where $\delta_0=\hat{X}_1-c\hat{X}_2$. The best choice for c minimizes $\Delta^2_{inf,L}\hat{X}$ and can be adjusted by experiment, or calculated as discussed in [11] to be $c=(\langle \hat{X}_1,\hat{X}_2\rangle)/\Delta^2\hat{X}_2$, where we define $\langle \hat{X}_1,\hat{X}_2\rangle=\langle \hat{X}_1\hat{X}_2\rangle-\langle \hat{X}_1\rangle\langle \hat{X}_2\rangle$.

Generally, the linear estimate will not be the best estimate for the outcome at A, based on the result at B. Therefore generally we have $\Delta_{inf,L}\hat{X}\geqslant\Delta_{inf}\hat{X}$ and $\Delta_{inf,L}\hat{Y}\geqslant\Delta_{inf}\hat{Y}$ [11]. The observation of

$$\Delta_{inf,L}\hat{X}_1\Delta_{inf,L}\hat{Y}_1 < 1 \tag{4.4}$$

will then also imply EPR correlations in the spirit of the EPR paradox.

B. An entanglement criterion based on the observation of two-mode squeezing

Entanglement may be deduced through a whole set of criteria, of which the EPR criterion (4.2) is one [11]. It is possible to deduce entanglement through other criteria [14] without the need to prove the strong EPR correlations. This has significance within quantum mechanics, but not necessarily the broader implications of the EPR criterion.

Such entanglement criteria, derived by Duan *et al.* and by Simon [14], are based on the proof of quantum inseparability, where the failure of a separable density matrix

$$\rho = \sum_R P_R\rho_R^1\rho_R^2 \tag{4.5}$$

($\Sigma_R P_R=1$) is proved. Particularly useful for our purposes is a criterion considered by Duan *et al.* sufficient to demonstrate entanglement (inseparability). We define

$$\delta\hat{X} = \hat{X}_1 - \hat{X}_2,$$

$$\delta\hat{Y} = \hat{Y}_1 + \hat{Y}_2. \tag{4.6}$$

Entanglement is guaranteed provided that the sum of the variances is bounded by

$$\Delta^2\delta\hat{X} + \Delta^2\delta\hat{Y} < 4. \tag{4.7}$$

This observation of this entanglement criterion (4.7) may be identified as a "two-mode squeezing" criterion for entanglement, since the individual criterion

$$\Delta^2\delta\hat{X} < 2 \tag{4.8}$$

is the criterion for the observation of a type of "two-mode squeezing." In this way we see that fields that are two-mode squeezed with respect to both X_1-X_2 and Y_1+Y_2, each satisfying Eq. (4.8), are necessarily entangled.

C. EPR correlations of the nondegenerate parametric system

The EPR correlations and entanglement were originally predicted for the outputs of the nondegenerate parametric oscillator [10]. For intracavity entanglement, we define the quadrature phase amplitudes

$$\hat{X}_1 = (\hat{a}_1 + \hat{a}_1^\dagger),$$

$$\hat{Y}_1 = (\hat{a}_1 - \hat{a}_1^\dagger)/i,$$

$$\hat{X}_2 = (\hat{a}_2 + a_2^\dagger),$$

$$\hat{Y}_2 = (\hat{a}_2 - \hat{a}_2^\dagger)/i, \tag{4.9}$$

and identify correlated observables for the oscillator, so that X_1 is correlated with X_2 and Y_1 is correlated with $-Y_2$. The Heisenberg uncertainty relation for the orthogonal amplitudes of mode $\hat{a}_1$ is $\Delta^2X_1\Delta^2Y_1\geqslant 1$.

As explained in the previous section, for practical reasons

it is preferable to use the corresponding *output* quadratures defined at or near zero frequency, which are $\hat{X}_i^{out}, \hat{Y}_i^{out}$. However, the detailed arguments depend only on having the commutators defined above, together with the requirement of causality—that is, the observations must take place with spacelike separations between the two detectors over the whole observation period T.

We calculate several types of EPR or entanglement measures. First we evaluate the 1989 inferred HUP EPR criterion (4.2) but using the linear estimate form, which will allow demonstration of both entanglement and EPR correlations defined in the spirit of the original EPR paradox. In terms of quadrature phase amplitude measurements this strong criterion is satisfied when

$$\Delta^2_{inf,L}X^{out}\Delta^2_{inf,L}Y^{out} = \Delta^2(X_1^{out} - c_x X_2^{out})\Delta^2(Y_1^{out} - c_y Y_2^{out}) < 1. \tag{4.10}$$

Now $c_x = \langle X_1^{out}, X_2^{out}\rangle / \Delta^2 X_2^{out}$ and $c_y = \langle Y_1^{out}, Y_2^{out}\rangle / \Delta^2 Y_2^{out}$ will minimize [11] the inference variances. Substituting for c_x and c_y, we explicitly calculate

$$\Delta^2_{inf,L}X^{out} = \Delta^2 X_1^{out} - \langle X_1^{out}, X_2^{out}\rangle^2 / \Delta^2 X_2^{out} \tag{4.11}$$

and

$$\Delta^2_{inf,L}Y^{out} = \Delta^2 Y_1^{out} - \langle Y_1^{out}, Y_2^{out}\rangle^2 / \Delta^2 Y_2^{out}. \tag{4.12}$$

For our particular system moments we have $\langle a_1\rangle = \langle a_2\rangle = 0$ and symmetry between the a_1 and a_2 modes, so that

$$\Delta^2 X_1^{out} = \frac{1}{2}(V + V^{\pi/2}) \geqslant 1 \tag{4.13}$$

and

$$\langle X_1^{out}, X_2^{out}\rangle = \frac{1}{2}(V^0 - V^{\pi/2}). \tag{4.14}$$

The linear inference EPR criterion (4.4) is then equivalent to

$$\Delta^2_{inf,L}X^{out} = \frac{2V^0 V^{\pi/2}}{V^0 + V^{\pi/2}} < 1. \tag{4.15}$$

This criterion is not equivalent to (4.2) which is based on the conditionals, since the linear estimate may not be the best, in which case it is possible that (4.2) is satisfied while (4.10) is not, and we do not pick up EPR and entanglement where it exists. Nevertheless the criterion (4.15) is sufficient to prove EPR correlations and entanglement.

Second, we calculate the Duan *et al.* two-mode squeezing criterion (4.7) for entanglement. Written in terms of quadrature phase amplitude measurements, this becomes

$$V^{\pi/2} = \frac{1}{4}[\Delta^2(X_1^{out} - X_2^{out}) + \Delta^2(Y_1^{out} + Y_2^{out})] < 1. \tag{4.16}$$

This criterion was explicitly shown to be both sufficient and necessary for entanglement for the case of Gaussian states (for appropriately chosen quadratures), meaning that in this case it would pick up any entanglement present. Our system is not Gaussian, and while these criteria are still sufficient to imply entanglement, they may not be necessary.

It is always the case that for ideal squeezing both the linear EPR and the squeezed entanglement criteria are satisfied. Where one has additional loss, however, it is possible for the squeezed-entanglement criterion (4.16) to be satisfied but not the EPR criterion (4.10). Such situations have been studied by Bowen *et al.* [7]. Our situation is different again, due to the fact that the underlying quantum states undergo nonlinear fluctuations and are inherently non-Gaussian.

D. EPR correlations of two degenerate parametric oscillators

EPR correlations and entanglement can also be obtained from the outputs of two degenerate parametric oscillators [34]. This requires an additional interferometer, but it does allow the use of type I frequency conversion, which may be easier to obtain at some wavelengths. With this technique, there are two squeezed outputs $\hat{a}, \hat{b}$, which are then combined at a beam splitter to obtain the EPR correlated modes. The following choice of relative phases generates modes $\hat{a}_1, \hat{a}_2$ similar to those analyzed above for EPR and entanglement signatures:

$$\hat{a}_1 = (\hat{a} - i\hat{b})/\sqrt{2},$$

$$\hat{a}_2 = (\hat{a} + i\hat{b})/\sqrt{2}. \tag{4.17}$$

With this choice, we can immediately deduce the correspondence between the input and output quadratures:

$$\hat{X}_1^{out} = (\hat{X}_a + \hat{Y}_b)/\sqrt{2},$$

$$\hat{Y}_1^{out} = (\hat{Y}_a - \hat{X}_b)/\sqrt{2},$$

$$\hat{X}_2^{out} = (\hat{X}_a - \hat{Y}_b)/\sqrt{2},$$

$$\hat{Y}_2^{out} = (\hat{Y}_a + \hat{X}_b)/\sqrt{2}. \tag{4.18}$$

Next, suppose the input fields are independently squeezed, with reduced fluctuations in each $\hat{Y}_{a,b}$ quadrature. Calculating correlations between the outputs gives

$$V_{DG}^{\pi/2} = \frac{1}{4}[\Delta^2(X_1^{out} - X_2^{out}) + \Delta^2(Y_1^{out} + Y_2^{out})]$$

$$= \frac{1}{2}(\Delta^2 Y_a^{out} + \Delta^2 Y_b^{out}) < 1. \tag{4.19}$$

This demonstrates that having two degenerate squeezed inputs can also generate EPR correlations. We note, however, that having two squeezed inputs will always require two pump beams. Thus, in comparing the results with these two methods, it is essential to use a comparison in which the total input photon flux is identical. The equation that should be used to compare with the input flux equation (2.13) is then

$$I_{DG} = \frac{|\mathcal{E}_c|^2}{\gamma_0} = N_c \gamma_0, \tag{4.20}$$

where in this case I_{DG} is the total input flux used to drive both the degenerate down-conversion cavities, and γ_0 is the pump mode decay rate.

The degenerate and nondegenerate routes to EPR correlations and entanglement are equivalent only in the linearized approximation. In the situation treated in this paper where the fields and states have a non-Gaussian character, the two methods are generally inequivalent, as we show later.

V. BELOW-THRESHOLD INTRACAVITY MOMENTS

In this section we use perturbation methods to study the nondegenerate parametric oscillator beyond the linearized regime both in the fully quantum mechanical approach using positive P representation and in the semiclassical approach based on the Wigner function. In the positive P case the basic quantities investigated are correlations involving the *internal* complex quadrature operators [35], mapped into stochastic variables according to

$$X_0 = (\alpha_0 + \alpha_0^+), \quad Y_0 = \frac{1}{i}(\alpha_0 - \alpha_0^+),$$

$$X = (\alpha_1 + \alpha_2^+), \quad Y = \frac{1}{i}(\alpha_1 - \alpha_2^+),$$

$$X^+ = (\alpha_2 + \alpha_1^+), \quad Y^+ = \frac{1}{i}(\alpha_2 - \alpha_1^+). \tag{5.1}$$

In the truncated Wigner (semiclassical) case, we have a similar set with α_i^+ replaced by α_i^*. To avoid excessive notation we use the same symbols for the quadrature variables in the two cases, noting that in the semiclassical case $X^+ = X^*$ and $Y^+ = Y^*$.

For developing a systematic perturbation procedure, it proves convenient to define

$$\gamma_r = \gamma_0/\gamma, \ \mu = \mathcal{E}/\mathcal{E}_c, \ g = \frac{\chi}{\gamma\sqrt{2\gamma_r}}, \tag{5.2}$$

and to introduce the following scaled quadrature variables:

$$x_0 = g\sqrt{2\gamma_r} X_0,$$

$$y_0 = g\sqrt{2\gamma_r} Y_0,$$

$$x = gX,$$

$$y = gY,$$

$$x^+ = gX^+,$$

$$y^+ = gY^+. \tag{5.3}$$

In terms of the physics involved, the expansion parameter is proportional to the critical intracavity photon number N_c, since

$$g^2 = 1/(2\gamma_r N_c).$$

This can also be written in terms of the input photon flux requirement at threshold as

$$g^2 = \frac{\gamma}{4I_c}.$$

That is, a smaller g^2 indicates a lower nonlinearity and hence increasing input photon flux at threshold. We note here that in comparing these results with the degenerate OPO case, a higher total input flux is needed for the same value of the degenerate coupling parameter g_{DG}^2, if the standard definitions [21] are adopted. This is simply due to the fact that one must drive two degenerate cavities instead of one to get correlated outputs. Hence, for the purposes of comparing these two methods of generating correlated fields, we will make comparisons *at the same total input flux*. This implies that, for comparison purposes,

$$g_{DG}^2 = \frac{\gamma}{2I_c} = 2g^2.$$

In terms of these new variables, and a scaled time $\tau = \gamma t$, the equations for the quadratures are given as follows.

Positive P equations

$$dx_0 = -\gamma_r[x_0 - 2\mu + (xx^+ - yy^+)]d\tau,$$

$$dy_0 = -\gamma_r[y_0 + (xy^+ + yx^+)]d\tau,$$

$$dx = \left[-x + \frac{1}{2}(xx_0 + yy_0)\right]d\tau + \frac{g}{\sqrt{2}}[\sqrt{x_0 + iy_0}\,dw_1 + \sqrt{x_0 - iy_0}\,dw_2^+],$$

$$dy = \left[-y + \frac{1}{2}(xy_0 - yx_0)\right]d\tau - i\frac{g}{\sqrt{2}}[\sqrt{x_0 + iy_0}\,dw_1 - \sqrt{x_0 - iy_0}\,dw_2^+],$$

$$dx^+ = \left[-x^+ + \frac{1}{2}(x^+x_0 + y^+y_0)\right]d\tau + \frac{g}{\sqrt{2}}[\sqrt{x_0 + iy_0}\,dw_2 + \sqrt{x_0 - iy_0}\,dw_1^+],$$

$$dy^+ = \left[-y^+ + \frac{1}{2}(x^+y_0 - y^+x_0)\right]d\tau - i\frac{g}{\sqrt{2}}[\sqrt{x_0 + iy_0}\,dw_2 - \sqrt{x_0 - iy_0}\,dw_1^+], \tag{5.4}$$

where $\langle dw_1 dw_2\rangle = \langle dw_1^+ dw_2^+\rangle = d\tau$.

Semiclassical equations

$$dx_0 = -\gamma_r[x_0 - 2\mu + (xx^+ - yy^+)]d\tau + \sqrt{2}g\gamma_r[dw_0 + dw_0^*],$$

$$dy_0 = -\gamma_r[y_0 + (xy^+ + yx^+)]d\tau - i\sqrt{2}g\gamma_r[dw_0 - dw_0^*],$$

$$dx = \left[-x + \frac{1}{2}(xx_0 + yy_0)\right]d\tau + g[dw_1 + dw_2^*],$$

$$dy = \left[-y + \frac{1}{2}(xy_0 - yx_0) \right] d\tau - ig[dw_1 - dw_2^*],$$

$$dx^+ = \left[-x^+ + \frac{1}{2}(x^+x_0 + y^+y_0) \right] d\tau + g[dw_2 + dw_1^*],$$

$$dy^+ = \left[-y^+ + \frac{1}{2}(x^+y_0 - y^+x_0) \right] d\tau - ig[dw_2 - dw_1^*], \tag{5.5}$$

where $\langle dw_i dw_j^* \rangle = \delta_{ij} d\tau$.

In order to solve these coupled equations systematically, we introduce a formal perturbation expansion in powers of g:

$$x_k = \sum_{n=0}^{\infty} g^n x_k^{(n)},$$

$$y_k = \sum_{n=0}^{\infty} g^n y_k^{(n)}. \tag{5.6}$$

This expansion has the property that the zeroth order term corresponds to the large classical field of order $1/g$ in the unscaled quadratures, the first order term involves quantum fluctuations of order 1, and the higher order terms correspond to nonlinear corrections to the quantum fluctuations of order g and higher.

A. Matched power equations in the positive *P* representation

Substituting Eq. (5.6) in Eq. (5.4) and equating like powers of g on both sides, we obtain a hierarchy of stochastic equations. The set of equations thus obtained, if desired, can be diagrammatically analyzed using the "stochastic diagram" method [36]. The zeroth order equations are

$$dx_0^{(0)} = -\gamma_r[x_0^{(0)} - 2\mu + (x^{(0)}x^{+(0)} - y^{(0)}y^{+(0)})]d\tau,$$

$$dy_0^{(0)} = -\gamma_r[y_0^{(0)} + (x^{(0)}y^{+(0)} + y^{(0)}x^{+(0)})]d\tau,$$

$$dx^{(0)} = \left[-x^{(0)} + \frac{1}{2}(x^{(0)}x_0^{(0)} + y^{(0)}y_0^{(0)}) \right] d\tau,$$

$$dy^{(0)} = \left[-y^{(0)} + \frac{1}{2}(x^{(0)}y_0^{(0)} - y^{(0)}x_0^{(0)}) \right] d\tau,$$

$$dx^{+(0)} = \left[-x^{+(0)} + \frac{1}{2}(x^{+(0)}x_0^{(0)} + y^{+(0)}y_0^{(0)}) \right] d\tau,$$

$$dy^{+(0)} = \left[-y^{+(0)} + \frac{1}{2}(x^{+(0)}y_0^{(0)} - y^{+(0)}x_0^{(0)}) \right] d\tau. \tag{5.7}$$

These equations correspond to the classical nonlinear equations for the intracavity quadratures expressed in terms of dimensionless scaled fields. Below threshold, the steady-state solution of these equations is well known and is given by

$$x_0^{(0)} = 2\mu,$$

$$y_0^{(0)} = x^{(0)} = y^{(0)} = 0. \tag{5.8}$$

The first order equations are

$$dx_0^{(1)} = -\gamma_r x_0^{(1)} d\tau,$$

$$dy_0^{(1)} = -\gamma_r y_0^{(1)} d\tau,$$

$$dx^{(1)} = -(1-\mu)x^{(1)}d\tau + \sqrt{2\mu}dw_{x1},$$

$$dy^{(1)} = -(1+\mu)y^{(1)}d\tau - i\sqrt{2\mu}dw_{y1},$$

$$dx^{+(1)} = -(1-\mu)x^{+(1)}d\tau + \sqrt{2\mu}dw_{x2},$$

$$dy^{+(1)} = -(1+\mu)y^{+(1)}d\tau - i\sqrt{2\mu}dw_{y2}. \tag{5.9}$$

We have introduced new Wiener increments as $dw_{x1(y1)}(\tau) = [dw_1(\tau) \pm dw_2^+(\tau)]/\sqrt{2}$ and $dw_{x2(y2)}(\tau) = [dw_2(\tau) \pm dw_1^+(\tau)]/\sqrt{2}$, with the following correlations:

$$\langle dw_{x1} dw_{x2} \rangle = d\tau,$$

$$\langle dw_{y1} dw_{y2} \rangle = d\tau. \tag{5.10}$$

and all other correlations vanishing.

Equations (5.9) are the ones that are normally used to predict squeezing. They are linear stochastic equations with nonclassical Gaussian white noise and, if higher order corrections are ignored, yield an ideal squeezed state for the subharmonic quadratures together with an ideal coherent state for the pump. Further, from the structure of these equations, it is evident that the steady-state solution for the pump field quadratures, in this order, vanishes. We can, therefore, without loss of generality, set all odd orders of $x_0^{(n)}, y_0^{(n)}$ for the pump, and all even orders of $x_i^{(n)}, y_i^{(n)}$, $i=1,2$, for the signal and idler fields, respectively, equal to zero. With this in mind, the second order equations turn out to be

$$dx_0^{(2)} = -\gamma_r[x_0^{(2)} + x^{(1)}x^{+(1)} - y^{(1)}y^{+(1)}]d\tau,$$

$$dy_0^{(2)} = -\gamma_r[y_0^{(2)} + x^{(1)}y^{+(1)} + y^{(1)}x^{+(1)}]d\tau. \tag{5.11}$$

Since, in the present work, our primary interest is to calculate the first nonlinear corrections to ideal squeezed-state behavior, to be consistent, we need to include contributions from the third order equations as well. These equations are as given below:

$$dx^{(3)} = \left[-(1-\mu)x^{(3)} + \frac{1}{2}(x^{(1)}x_0^{(2)} + y^{(1)}y_0^{(2)}) \right] d\tau + \frac{1}{2\sqrt{2\mu}}[x_0^{(2)}dw_{x1} + iy_0^{(2)}dw_{y1}],$$

$$dy^{(3)} = \left[-(1+\mu)y^{(3)} + \frac{1}{2}(x^{(1)}y_0^{(2)} - x_0^{(2)}y^{(1)}) \right] d\tau + \frac{1}{2\sqrt{2\mu}}[y_0^{(2)}dw_{x1} - ix_0^{(2)}dw_{y1}],$$

$$dx^{+(3)} = \left[-(1-\mu)x^{+(3)} + \frac{1}{2}(x^{+(1)}x_0^{(2)} + y^{+(1)}y_0^{(2)}) \right] d\tau + \frac{1}{2\sqrt{2\mu}}[x_0^{(2)}dw_{x2} + iy_0^{(2)}dw_{y2}],$$

$$dy^{+(3)} = \left[-(1+\mu)y^{+(3)} + \frac{1}{2}(x^{+(1)}y_0^{(2)} - x_0^{(2)}y^{+(1)}) \right] d\tau + \frac{1}{2\sqrt{2\mu}}[y_0^{(2)}dw_{x2} - ix_0^{(2)}dw_{y2}]. \quad (5.12)$$

This set of equations has nontrivial noise terms as they depend on the solutions of the stochastic equations at second order.

B. Operator moments in the positive *P* representation

The set of stochastic equations together with the Itô rules for variable changes [28] permit computation of the operator moments in a straightforward manner. Apart from their intrinsic interest, they are useful in checking the correctness of somewhat more involved spectral calculations given later. The results obtained are summarized below:

$$\langle x_0^{(2)} \rangle = \frac{-2\mu^2}{1-\mu^2},$$

$$\langle y^{(1)}y^{+(1)} \rangle = -\left(\frac{\mu}{1+\mu} \right),$$

$$\langle x^{(1)}x^{+(1)} \rangle = \left(\frac{\mu}{1-\mu} \right),$$

$$\langle y^{(1)}y^{+(3)} \rangle = \frac{\mu}{4(1+\mu)(1-\mu^2)} \times \left[\frac{\mu\gamma_r}{\gamma_r+2} + \frac{\gamma_r(2-\mu+\mu^2)+4(1+\mu)}{(1+\mu)[\gamma_r+2(1+\mu)]} \right],$$

$$\langle x^{(1)}y^{+(1)}y_0^{(2)} \rangle = \frac{\mu^2}{1-\mu^2}\left(\frac{\gamma_r}{\gamma_r+2} \right). \quad (5.13)$$

The first quantity above pertains to the depletion of the pump that supplies energy for the subharmonic mode. The next two quantities are the squeezed and enhanced quadratures as given by the linearized theory, while the fourth one is the first correction to the linearized theory. The last one is the steady-state triple quadrature correlation. This quantity has been investigated earlier for its relevance in distinguishing quantum mechanics from a local hidden variable theory [37].

The results above yield the following expression for the steady-state intracavity squeezed quadrature fluctuations:

$$\langle \hat{Y}\hat{Y}^\dagger \rangle_{ss} = 1 + \langle :\hat{Y}\hat{Y}^\dagger: \rangle = \frac{1}{1+\mu} + \frac{g^2\mu}{2(1+\mu)(1-\mu^2)}\left[\frac{\mu\gamma_r}{\gamma_r+2} + \frac{\gamma_r(2-\mu+\mu^2)+4(1+\mu)}{(1+\mu)[\gamma_r+2(1+\mu)]} \right]. \quad (5.14)$$

Noting that $g_{DG}^2 = 2g^2$ at the same total flux input, we can now compare the degenerate and nondegenerate routes to obtaining EPR correlations. By comparison, the degenerate OPO yields quite different nonlinear corrections [21] near threshold:

$$\langle \hat{Y}_{DG}^2 \rangle = \frac{1}{1+\mu} + \frac{2g^2\mu}{2(1+\mu)(1-\mu^2)}\left[\frac{\mu\gamma_r}{\gamma_r+2} + \frac{\gamma_r(1-\mu+\mu^2)+2(1+\mu)}{(1+\mu)[\gamma_r+2(1+\mu)]} \right]. \quad (5.15)$$

For the same total photon flux input and damping ratio γ_r, the nonlinear corrections are always larger for the degenerate case, as compared to the nondegenerate case. In the limit of $\gamma_r \to 0$, the nonlinear corrections are equivalent in the two cases. Questions relating to optimal output entanglement and squeezing will be treated in the next section, using frequency-domain methods.

The triple moment correlation for the quadratures scales with $1/\sqrt{N_c}$ and increases with driving field, since it is given by

$$\langle \hat{X}\hat{Y}^\dagger\hat{Y}_0 \rangle = \frac{g\mu^2}{1-\mu^2}\left(\frac{\sqrt{\gamma_r/2}}{\gamma_r+2} \right). \quad (5.16)$$

C. Matched power equations in semiclassical theory

Using the same technique of matching the powers of g, we obtain the following set of equations in the semiclassical theory. The zeroth order equation are

$$dx_0^{(0)} = -\gamma_r[x_0^{(0)} - 2\mu + (x^{(0)}x^{+(0)} - y^{(0)}y^{+(0)})]d\tau,$$

$$dy_0^{(0)} = -\gamma_r[y_0^{(0)} + (x^{(0)}y^{+(0)} + y^{(0)}x^{+(0)})]d\tau,$$

$$dx^{(0)} = \left[-x^{(0)} + \frac{1}{2}(x^{(0)}x_0^{(0)} + y^{(0)}y_0^{(0)}) \right] d\tau,$$

$$dy^{(0)} = \left[-y^{(0)} + \frac{1}{2}(x^{(0)}x_0^{(0)} - y^{(0)}x_0^{(0)}) \right] d\tau,$$

$$dx^{+(0)} = \left[-x^{+(0)} + \frac{1}{2}(x^{+(0)}x_0^{(0)} + y^{+(0)}y_0^{(0)}) \right] d\tau,$$

$$dy^{+(0)} = \left[-y^{+(0)} + \frac{1}{2}(x^{+(0)}y_0^{(0)} - y^{+(0)}x_0^{(0)}) \right] d\tau. \quad (5.17)$$

As in the positive *P* case, the steady-state solution of these equations is given by

$$x_0^{(0)} = 2\mu,$$

$$y_0^{(0)} = x^{(0)} = y^{(0)} = 0. \tag{5.18}$$

The first order equations aren

$$\begin{aligned}
dx_0^{(1)} &= -\gamma_r x_0^{(1)} d\tau + 2\gamma_r dw_{x0},\\
dy_0^{(1)} &= -\gamma_r y_0^{(1)} d\tau + 2\gamma_r dw_{y0},\\
dx^{(1)} &= -(1-\mu)x^{(1)} d\tau + \sqrt{2} dw_{x1},\\
dy^{(1)} &= -(1+\mu)y^{(1)} d\tau + \sqrt{2} dw_{y1},\\
dx^{+(1)} &= -(1-\mu)x^{+(1)} d\tau + \sqrt{2} dw_{x2},\\
dy^{+(1)} &= -(1+\mu)y^{+(1)} d\tau + \sqrt{2} dw_{y2},
\end{aligned} \tag{5.19}$$

where

$$\langle dw_{x0} dw_{x0}\rangle = \langle dw_{y0} dw_{y0}\rangle = \langle dw_{x1} dw_{x2}\rangle = \langle dw_{y1} dw_{y2}\rangle = d\tau, \tag{5.20}$$

with all other correlations vanishing.

The equations above give the linearized theory. The first nonlinear corrections come from the next two sets of equations given below.

The second order equations are:

$$\begin{aligned}
dx_0^{(2)} &= -\gamma_r [x_0^{(2)} + x^{(1)}x^{+(1)} - y^{(1)}y^{+(1)}] d\tau,\\
dy_0^{(2)} &= -\gamma_r [y_0^{(2)} + x^{(1)}y^{+(1)} + y^{(1)}x^{+(1)}] d\tau,\\
dx^{(2)} &= \left[-(1-\mu)x^{(2)} + \frac{1}{2}(x^{(1)}x_0^{(1)} + y^{(1)}y_0^{(1)}) \right] d\tau,\\
dy^{(2)} &= \left[-(1+\mu)y^{(2)} + \frac{1}{2}(x^{(1)}y_0^{(1)} - x_0^{(1)}y^{(1)}) \right] d\tau,\\
dx^{+(2)} &= \left[-(1-\mu)x^{+(2)} + \frac{1}{2}(y^{+(1)}y_0^{(1)} + x^{+(1)}x_0^{(1)}) \right] d\tau,\\
dy^{+(2)} &= \left[-(1+\mu)y^{+(2)} + \frac{1}{2}(x^{+(1)}y_0^{(1)} - x_0^{(1)}y^{+(1)}) \right] d\tau.
\end{aligned} \tag{5.21}$$

The third order equations are

$$\begin{aligned}
dx_0^{(3)} &= -\gamma_r [x_0^{(3)} + x^{(1)}x^{+(2)} + x^{(2)}x^{+(1)} - y^{(1)}y^{+(2)} - y^{(2)}y^{+(1)}] d\tau,\\
dy_0^{(3)} &= -\gamma_r [y_0^{(3)} + x^{(1)}y^{+(2)} + x^{(2)}y^{+(1)} + y^{(1)}x^{+(2)} + y^{(2)}x^{+(1)}] d\tau,\\
dx^{(3)} &= \left[-(1-\mu)x^{(3)} + \frac{1}{2}(x^{(1)}x_0^{(2)} + x^{(2)}x_0^{(1)} + y^{(1)}y_0^{(2)} + y^{(2)}y_0^{(1)}) \right] d\tau,\\
dy^{(3)} &= \left[-(1+\mu)y^{(3)} + \frac{1}{2}(x^{(1)}y_0^{(2)} + x^{(2)}y_0^{(1)} - y^{(1)}x_0^{(2)} - y^{(2)}x_0^{(1)}) \right] d\tau,\\
dx^{+(3)} &= \left[-(1-\mu)x^{+(3)} + \frac{1}{2}(x^{+(1)}x_0^{(2)} + x^{+(2)}x_0^{(1)} + y^{+(1)}y_0^{(2)} + y^{+(2)}y_0^{(1)}) \right] d\tau,\\
dy^{+(3)} &= \left[-(1+\mu)y^{+(3)} + \frac{1}{2}(x^{+(1)}y_0^{(2)} + x^{+(2)}y_0^{(1)} - y^{+(1)}x_0^{(2)} - y^{+(2)}x_0^{(1)}) \right] d\tau.
\end{aligned} \tag{5.22}$$

D. Operator moments in semiclassical theory

In this case, the analogs of the results in Eq. (5.13) are found to be

$$\begin{aligned}
\langle x_0^{(2)}\rangle &= \frac{-2\mu^2}{1-\mu^2},\\
\langle x^{(1)}x^{+(1)}\rangle &= \left(\frac{1}{1-\mu}\right),\\
\langle y^{(1)}y^{+(1)}\rangle &= \left(\frac{1}{1+\mu}\right),\\
\langle y^{(2)}y^{+(2)}\rangle &= \frac{1}{2(1-\mu)(1+\mu)}\left(\frac{\gamma_r}{\gamma_r+2}\right) + \frac{1}{2(1+\mu)^2}\left(\frac{\gamma_r}{\gamma_r+2(1+\mu)}\right),\\
\langle y^{(1)}y^{+(3)}\rangle &= -\frac{\mu}{4(1-\mu)(1+\mu)^2}\left(\frac{\gamma_r}{\gamma_r+2}\right) + \frac{\mu}{2(1-\mu)(1+\mu)^3} + \frac{\mu}{4(1+\mu)^3}\left[\frac{\gamma_r}{\gamma_r+2(1+\mu)}\right],\\
\langle x^{(1)}y^{+(1)}y_0^{(2)}\rangle &+ \langle x^{(2)}y^{+(1)}y_0^{(1)}\rangle + \langle x^{(1)}y^{+(2)}y_0^{(1)}\rangle = \frac{1}{1-\mu^2}\left(\frac{\gamma_r}{\gamma_r+2}\right).
\end{aligned} \tag{5.23}$$

The main difference in these calculation, compared with the positive P results, appears in the nonlinear correction for the subharmonic squeezed quadrature. Up to second order in g we have

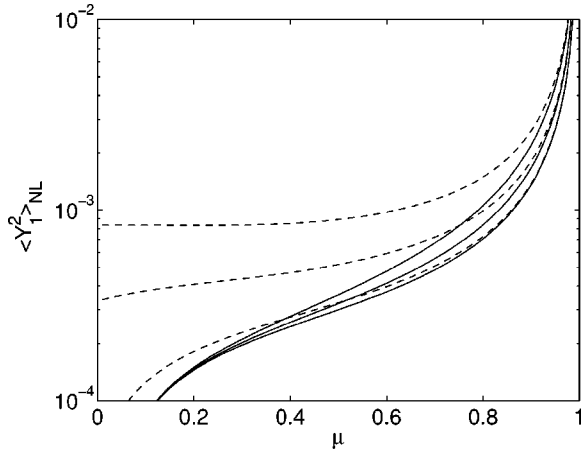

FIG. 2. Graph of second order nonlinear correction to the squeezing/entanglement moment $\langle \hat{Y}_1^2 \rangle_{NL}$ vs driving field μ, using parameters of $g^2=0.001$ and $\gamma_r=0.1$, 1, 10. Upper lines have larger γ_r values. Solid lines are the positive P results, which vanish at small driving field. Dotted lines are the (less accurate) semiclassical results, which do not vanish at small driving field.

$$\langle \hat{Y}\hat{Y}^{+}\rangle = \frac{1}{g^2}[g^2\langle y^{(1)}y^{+(1)}\rangle + g^4\langle y^{(2)}y^{+(2)}\rangle + 2g^4\langle y^{(1)}y^{+(3)}\rangle]$$
$$= \frac{1}{1+\mu} + \frac{g^2}{2(1+\mu)(1-\mu^2)}\left[\frac{\gamma_r}{\gamma_r+2} + \frac{\gamma_r(1+3\mu-2\mu^2)+4\mu(1+\mu)}{(1+\mu)[\gamma_r+2(1+\mu)]}\right]. \quad (5.24)$$

The similarities and disagreement between this result and the positive P expression for the same quantity deserve further comments, given in the concluding section. In particular, we note that, while the linear terms agree, the nonlinear terms are not in agreement below threshold. However, just below threshold the two theories give essentially identical nonlinear corrections. There is good agreement also in the limit $\gamma_r \to 0$.

In the case of the triple moments, the discrepancy appears to leading order, since the truncated Wigner theory predicts that

$$\langle \hat{X}\hat{Y}^{\dagger}\hat{Y}_0\rangle = \frac{g}{1-\mu^2}\left(\frac{\sqrt{\gamma_r/2}}{\gamma_r+2}\right). \quad (5.25)$$

Here the semiclassical prediction is for a moment that is independent of input power as $\mu \to 0$, which is physically unacceptable (since one expects a vacuum state in this limit), and inconsistent with the full quantum result of the positive P theory, in Eq. (5.16).

Comparisons of the positive P and truncated Wigner squeezing moments are shown in Fig. 2.

VI. POSITIVE *P* SPECTRAL CORRELATIONS

Next, we proceed to analyze spectral correlations which are of direct relevance to comparison with experiments. In particular, we compute the nonlinear corrections to the squeezing spectrum using the positive P stochastic variables.

A. Fourier transforms

To perform calculations in the frequency domain, it proves convenient to deal directly with the Fourier transforms

$$\tilde{x}(\Omega) = \int \frac{d\tau}{\sqrt{2\pi}} e^{i\Omega\tau} x(\tau)$$

of the hierarchy of the stochastic equations obtained earlier. The equations thus obtained contain noise terms

$$\xi_{x,y}(\Omega) = \int \frac{d\tau}{\sqrt{2\pi}} e^{i\Omega\tau} \xi_{x,y}(\tau)$$

with the following correlations:

$$\langle \xi_a(\Omega)\rangle = 0,$$

$$\langle \xi_{a1}(\Omega)\xi_{b2}(\Omega')\rangle = \delta_{ab}\delta(\Omega+\Omega'). \quad (6.1)$$

In this context, for notational compactness it is useful to introduce the standard notation for convolution of two functions:

$$[A * B](\Omega) = \int \frac{d\Omega'}{\sqrt{2\pi}} A(\Omega')B(\Omega-\Omega').$$

With this in mind, the stochastic equations obtained earlier may be rewritten in the frequency domain as follows.

First order

$$\tilde{x}^{(1)}(\Omega) = \frac{\sqrt{2\mu}\xi_{x1}(\Omega)}{(-i\Omega+1-\mu)},$$

$$\tilde{y}^{(1)}(\Omega) = -\frac{i\sqrt{2\mu}\xi_{y1}(\Omega)}{(-i\Omega+1+\mu)},$$

$$\tilde{x}^{+(1)}(\Omega) = \frac{\sqrt{2\mu}\xi_{x2}(\Omega)}{(-i\Omega+1-\mu)},$$

$$\tilde{y}^{+(1)}(\Omega) = -\frac{i\sqrt{2\mu}\xi_{y2}(\Omega)}{(-i\Omega+1+\mu)}. \quad (6.2)$$

Second order

$$\tilde{x}_0^{(2)}(\Omega) = -\frac{\gamma_r[\tilde{x}^{(1)} * \tilde{x}^{+(1)} - \tilde{y}^{(1)} * \tilde{y}^{+(1)}](\Omega)}{(-i\Omega+\gamma_r)},$$

$$\tilde{y}_0^{(2)}(\Omega) = -\frac{\gamma_r[\tilde{x}^{(1)} * \tilde{y}^{+(1)} + \tilde{x}^{+(1)} * \tilde{y}^{(1)}](\Omega)}{(-i\Omega+\gamma_r)}. \quad (6.3)$$

Third order

$$\tilde{x}^{(3)}(\Omega) = \frac{[\tilde{x}_0^{(2)} * (\tilde{x}^{(1)} + \xi_{x1}/\sqrt{2\mu}) + \tilde{y}_0^{(2)} * (\tilde{y}^{(1)} + i\xi_{y1}/\sqrt{2\mu})](\Omega)}{2(-i\Omega + 1 - \mu)},$$

$$\tilde{y}^{(3)}(\Omega) = \frac{[\tilde{y}_0^{(2)} * (\tilde{x}^{(1)} + \xi_{x1}/\sqrt{2\mu}) - \tilde{x}_0^{(2)} * (\tilde{y}^{(1)} + i\xi_{y1}/\sqrt{2\mu})](\Omega)}{2(-i\Omega + 1 + \mu)},$$

$$\tilde{x}^{+(3)}(\Omega) = \frac{[\tilde{x}_0^{(2)} * (\tilde{x}^{+(1)} + \xi_{x2}/\sqrt{2\mu}) + \tilde{y}_0^{(2)} * (\tilde{y}^{+(1)} + i\xi_{y2}/\sqrt{2\mu})](\Omega)}{2(-i\Omega + 1 - \mu)},$$

$$\tilde{y}^{+(3)}(\Omega) = \frac{[\tilde{y}_0^{(2)} * (\tilde{x}^{+(1)} + \xi_{x2}/\sqrt{2\mu}) - \tilde{x}_0^{(2)} * (\tilde{y}^{+(1)} + i\xi_{y2}/\sqrt{2\mu})](\Omega)}{2(-i\Omega + 1 + \mu)}. \quad (6.4)$$

B. Output correlation spectrum

The output spectral features are obtained by calculating internal spectra, then transforming to the external correlation spectra.

1. Internal spectrum

We first calculate the internal spectrum of the squeezed field, which is given by $\langle \tilde{y}(\Omega_1)\tilde{y}^{+}(\Omega_2)\rangle$:

$$\langle \tilde{y}(\Omega_1)\tilde{y}^{+}(\Omega_2)\rangle = g^2\langle \tilde{y}^{(1)}(\Omega_1)\tilde{y}^{+(1)}(\Omega_2)\rangle + g^4\big[\langle \tilde{y}^{(1)}(\Omega_1)\tilde{y}^{+(3)} \times(\Omega_2)\rangle + \langle \tilde{y}^{(3)}(\Omega_1)\tilde{y}^{+(1)}(\Omega_2)\rangle\big] + \cdots. \quad (6.5)$$

The lowest order contribution is the usual result of the linearized theory and is given by

$$\langle \tilde{y}^{(1)}(\Omega_1)\tilde{y}^{+(1)}(\Omega_2)\rangle = -\frac{2\mu\delta(\Omega_1+\Omega_2)}{[\Omega_1^2 + (1+\mu)^2]}. \quad (6.6)$$

In terms of the squeezing variance, this means that

$$V^{(1)\pi/2}(\Omega) = 1 - \frac{4\mu}{\Omega^2 + (1+\mu)^2}. \quad (6.7)$$

For comparison, note that the complementary (unsqueezed) spectrum to this order is

$$\langle \tilde{x}^{(1)}(\Omega_1)\tilde{x}^{+(1)}(\Omega_2)\rangle = \frac{2\mu\delta(\Omega_1+\Omega_2)}{[\Omega_1^2 + (1-\mu)^2]}. \quad (6.8)$$

Taking the next order corrections into account, we find that the normally ordered internal spectral correlations of the squeezed quadrature are given by

$$\langle :\hat{Y}(\Omega_1)\hat{Y}^{\dagger}(\Omega_2):\rangle = \Bigg\{ \frac{-2\mu}{\Omega^2 + (1+\mu)^2} + \frac{2g^2\mu^2\gamma_r}{[\Omega^2 + (1+\mu)^2]^2} \times \Bigg[\frac{(\Omega^2 + 1 - \mu^2)}{\mu\gamma_r(1-\mu^2)} + \frac{(1-\mu+\gamma_r)(1+\mu) - \Omega^2}{(1-\mu)[\Omega^2 + (1-\mu+\gamma_r)^2]} - \frac{(1+\mu+\gamma_r)(1+\mu) - \Omega^2}{(1+\mu)[\Omega^2 + (1+\mu+\gamma_r)^2]} \Bigg] + O(g^4) \Bigg\} \delta(\Omega_1 + \Omega_2). \quad (6.9)$$

The correctness of the above expression can be checked by verifying the following equality:

$$\langle y^{(1)}(\tau)y^{+(3)}(\tau)\rangle_{ss} = \int \frac{d\Omega_1}{\sqrt{2\pi}} \int \frac{d\Omega_2}{\sqrt{2\pi}} e^{i(\Omega_1+\Omega_2)\tau} \times \langle \tilde{y}^{(1)}(\Omega_1)\tilde{y}^{+(3)}(\Omega_2)\rangle. \quad (6.10)$$

2. Entanglement and external spectrum

The corresponding external squeezing spectrum is then

$$V^{\pi/2}(\Omega) = 1 - \frac{4\mu}{\Omega^2 + (1+\mu)^2} + \frac{4g^2\mu^2\gamma_r}{[\Omega^2 + (1+\mu)^2]^2} \times \Bigg[\frac{(\Omega^2 + 1 - \mu^2)}{\mu\gamma_r(1-\mu^2)} + \frac{(1-\mu+\gamma_r)(1+\mu) - \Omega^2}{(1-\mu)[\Omega^2 + (1-\mu+\gamma_r)^2]} - \frac{(1+\mu+\gamma_r)(1+\mu) - \Omega^2}{(1+\mu)[\Omega^2 + (1+\mu+\gamma_r)^2]} \Bigg] + O(g^4). \quad (6.11)$$

This equation gives the complete squeezing spectrum, including all nonlinear corrections to order g^2 or $1/N_c$. The linear part gives perfect squeezing for $\mu=1$ and $\Omega=0$, as expected from the linear theory.

Once again, we can compare these results with those for the degenerate route to obtaining EPR correlations, at the same total input flux. The external squeezing spectrum is then

$$V_{DG}^{\pi/2}(\Omega) = 1 - \frac{4\mu}{\Omega^2 + (1+\mu)^2} + \frac{8g^2\mu^2\gamma_r}{[\Omega^2 + (1+\mu)^2]^2} \times \Bigg[\frac{(\Omega^2 + 1 - \mu^2)}{2\mu\gamma_r(1-\mu^2)} + \frac{(1-\mu+\gamma_r)(1+\mu) - \Omega^2}{(1-\mu)[\Omega^2 + (1-\mu+\gamma_r)^2]} - \frac{(1+\mu+\gamma_r)(1+\mu) - \Omega^2}{(1+\mu)[\Omega^2 + (1+\mu+\gamma_r)^2]} \Bigg]. \quad (6.12)$$

The nonlinear terms give corrections to perfect squeezing below threshold. Just as was found for the total squeezing

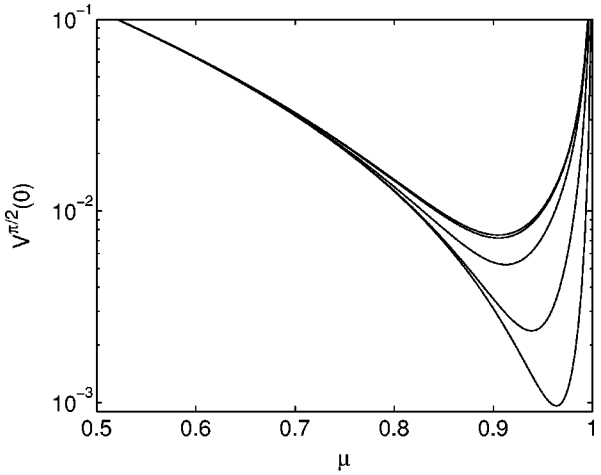

FIG. 3. Optimum squeezing with $g^2=0.001$, $\gamma_r=10^{-3}$, 10^{-2}, 10^{-1}, 1, 10. Higher lines have larger values of γ_r. Here, $V^{\pi/2}<1$ indicates squeezing and entanglement occurring at zero frequency.

moments, the nonlinear spectral corrections at the same total input flux are always smaller using a nondegenerate OPO as opposed to using a pair of degenerate OPO's.

At zero frequency, we find that

$$V^{\pi/2}(0) = 1 - \frac{4\mu}{(1+\mu)^2} + \frac{4g^2\mu}{(1+\mu)^4} \times\left[1 + \frac{2\mu^2\gamma_r(2+\gamma_r)}{(1-\mu)[(1+\gamma_r)^2-\mu^2]}\right]. \quad (6.13)$$

The resulting behavior for the optimum entanglement, which is found at zero frequency (ignoring complications from technical noise), is shown in Fig. 3. We see that, as expected, the entanglement is not optimized at the critical point, since the nonlinear critical fluctuations spoil this before an ideal entangled two-mode squeezed state with $V^{\pi/2}=0$ is achieved. Better entanglement is obtained when γ_r is reduced, as this minimizes the "information leakage" in the losses of the pump mode. In this limit, the only losses are through the signal and idler output ports, which are needed in order to have extracavity measurements.

This expression does not describe the spectrum very close to the critical point, as it diverges at the threshold. This region requires a different kind of scaling and is discussed later.

3. Unsqueezed spectrum

The complementary or unsqueezed spectrum contains critical fluctuations which grow extremely large near threshold. For measurements of the maximum quadrature fluctuations, this is given by

$$V^0(\Omega) = 1 + \frac{4\mu}{\Omega^2+(1-\mu)^2} - \frac{4g^2\mu^2\gamma_r}{[\Omega^2+(1-\mu)^2]^2} \times\left[\frac{(\Omega^2+1-\mu^2)}{\mu\gamma_r(1-\mu^2)} + \frac{(1-\mu+\gamma_r)(1-\mu)-\Omega^2}{(1-\mu)[\Omega^2+(1-\mu+\gamma_r)^2]} - \frac{(1+\mu+\gamma_r)(1-\mu)-\Omega^2}{(1+\mu)[\Omega^2+(1+\mu+\gamma_r)^2]}\right]. \quad (6.14)$$

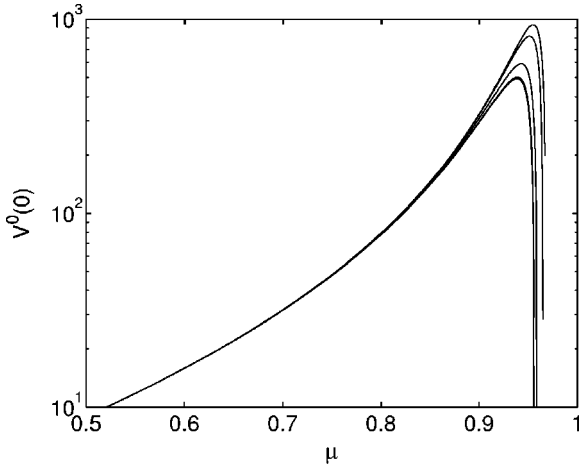

FIG. 4. Complementary (unsqueezed) spectrum with $g^2=0.001$, $\gamma_r=10^{-3}$, 10^{-2}, 10^{-1}, 1, 10. Lower lines have larger values of γ_r.

The resulting behavior for the zero-frequency critical fluctuations is shown in Fig. 4. Near the critical point, higher order terms are likely to become significant. The effects of these are treated in the next section.

4. Heisenberg uncertainty principle

We note here that in the linearized analysis the product of these spectra corresponds to the Heisenberg uncertainty principle:

$$V^0(\Omega)V^{\pi/2}(\Omega) = \left[1 - \frac{4\mu}{\Omega^2+(1+\mu)^2}\right]\left[1 + \frac{4\mu}{\Omega^2+(1-\mu)^2}\right] = 1. \quad (6.15)$$

Near threshold where nonlinear effects are dominant, this relationship no longer holds. The zero-frequency nonlinear uncertainty product is shown in Fig. 5. Just below the critical point, the nonlinear corrections apparently predict an uncertainty product less than unity, which clearly implies that the second order perturbation method breaks down here. An unexpected feature of these results is that for $\gamma_r \ll 1$ the uncer-

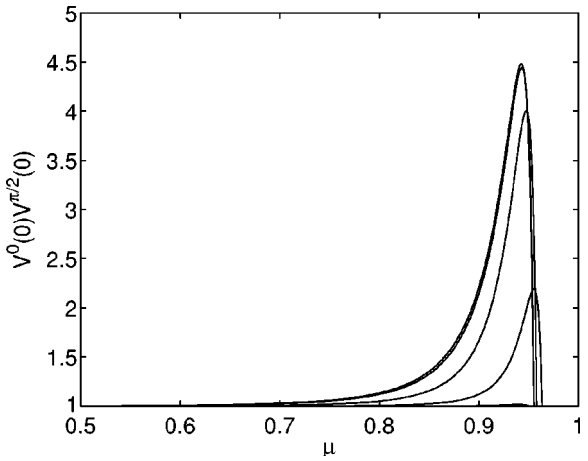

FIG. 5. Heisenberg uncertainty product with $g^2=0.001$, $\gamma_r=10^{-3}$, 10^{-2}, 10^{-1}, 1, 10. Higher lines have larger values of γ_r.

tainty product remains close to unity for all driving fields, indicating that there is a near-minimum uncertainty state for low frequency spectral measurements in the output fields. This does not mean that there is a minimum uncertainty state for the internal quadrature moments, since these are effectively integrated over all frequencies, and involve different quantum fields.

5. EPR paradox

We also investigate the behavior of the *inferred* Heisenberg uncertainty product, which demonstrates that there is an EPR paradox. In the original proposal, this uncertainty product would be zero, as the original EPR paradox involved perfect correlations. Instead, the minimum value of this product is determined by the nonlinear critical fluctuations. Due to symmetry, we need plot only the behavior of $\Delta^2_{inf,L}X^0$ in Fig. 6, using Eq. (4.15) for the inferred variance in terms of the squeezed and unsqueezed spectral variances given by Eqs. (6.11) and (6.14).

This shows qualitatively similar behavior to the entanglement measure based on squeezing, and in fact for strong entanglement the inferred uncertainty and squeezing measures are simply related by

$$\Delta^2_{inf,L}X^0 = 2V^{\pi/2}. \tag{6.16}$$

We see that near threshold the EPR measure and squeezing entanglement measure both show the existence of a strongly entangled output beam, as one might expect. The perturbation theory breaks down past the point where optimum entanglement is achieved, just below threshold, as we will show from direct numerical simulations.

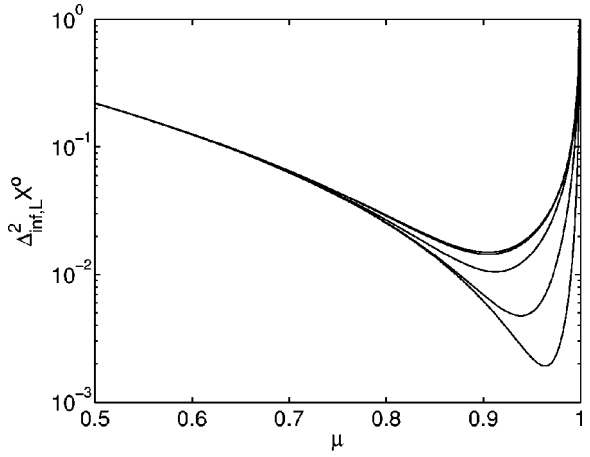

FIG. 6. Inferred quadrature uncertainty with $g^2=0.001$, $\gamma_r=10^{-3}$, 10^{-2}, 10^{-1}, 1, 10. Higher lines have larger values of γ_r. When $\Delta^2_{inf,L}X^0<1$, one may infer an EPR paradox.

C. Triple spectral correlations

Triple spectral correlations give quantum effects which distinguish very strongly [37] between the full quantum theory and the semiclassical approximation.

Here, we calculate the internal quadrature triple spectral correlation $\langle\tilde{x}(\Omega_1)\tilde{y}^+(\Omega_2)\tilde{y}_0(\Omega_3)\rangle$. To the lowest nonvanishing order this is given by

$$\langle\tilde{x}(\Omega_1)\tilde{y}^+(\Omega_2)\tilde{y}_0(\Omega_3)\rangle = g^4\langle\tilde{x}^{(1)}(\Omega_1)\tilde{y}^{+(1)}(\Omega_2)\tilde{y}_0^{(2)}(\Omega_3)\rangle. \tag{6.17}$$

Substituting for $\tilde{y}_0^{(2)}$, we have

$$\langle\tilde{x}^{(1)}(\Omega_1)\tilde{y}^{+(1)}(\Omega_2)\tilde{y}_0^{(2)}(\Omega_3)\rangle = -\frac{\gamma_r\langle\tilde{x}^{(1)}(\Omega_1)\tilde{y}^{+(1)}(\Omega_2)[\tilde{x}^{(1)}*\tilde{y}^{+(1)}+\tilde{x}^{+(1)}*\tilde{y}^{(1)}](\Omega_3)\rangle}{(-i\Omega_3+\gamma_r)}, \tag{6.18}$$

and using the Gaussian nature of the stochastic variables involved to factorize the fourth order correlations we obtain

$$\langle\hat{X}(\Omega_1)\hat{Y}^\dagger(\Omega_2)\hat{Y}_0(\Omega_3)\rangle = \frac{2g\mu^2\sqrt{\gamma_r}(\gamma_r+i\Omega_3)\delta(\Omega_1+\Omega_2+\Omega_3)}{\sqrt{\pi}[\Omega_3^2+\gamma_r^2][\Omega_1^2+(1-\mu)^2][\Omega_2^2+(1+\mu)^2]}. \tag{6.19}$$

To check this result, we can evaluate the steady-state triple moment by integrating over all frequencies, and find that we obtain the same result as given earlier by direct calculations in Eq. (5.16). This result will be compared later with the corresponding result obtained in the semiclassical theory.

D. Comparisons with simulations

In order to verify the accuracy of these analytic calculations, we performed extensive numerical simulations of the full nonlinear stochastic simulations, using a differencing technique as in earlier studies. We calculate only the nonlinear squeezing variance, defined as

$$V(\Omega) = V^{\pi/2}(\Omega) - V^{(1)\pi/2}(\Omega). \tag{6.20}$$

This allows us to focus on the nonlinear corrections, which are relatively small except very near the critical threshold at $\mu=1$. The numerical method has the advantage that, unlike perturbation theory, it is valid at all driving fields—even at the critical point.

The integration parameters used were step size $d\tau=0.001$, with a time window of $\tau_{max}=10\,000$. The number of stochastic trajectories used for averaging was 2000, resulting in typical relative sampling errors of around ±2%, as can be

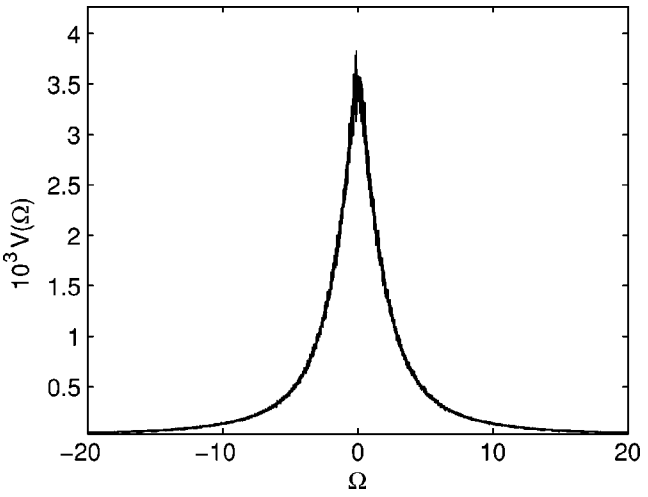

FIG. 7. Nonlinear squeezing spectrum with $g^2=0.005$, $\gamma_r=1$, and $\mu=0.5$. The dashed line represents the analytical result and the noisy line the stochastic simulation.

seen from the background sampling noise in some of the resulting spectra.

Typical results are shown in Figs. 7 and 8 below, for driving fields of $\mu=0.5, 0.9$. Note that these graphs include only the nonlinear corrections. Excellent agreement is found with the analytically predicted results for these values of the driving field.

Figure 9 shows results slightly closer to threshold, at $\mu=0.93$, which is the optimum driving field for the parameters chosen.

At this point, a maximum error in the analytic result of around 10^{-4} is found, due to the neglect of higher order nonlinear corrections. This indicates that the analytic perturbation theory is able to correctly predict nonlinear effects up to the optimum squeezing point, but starts to diverge beyond this point. The numerical results, however, are stable throughout the critical region. To obtain analytic predictions in the critical region, we turn to a different asymptotic expansion in a later section.

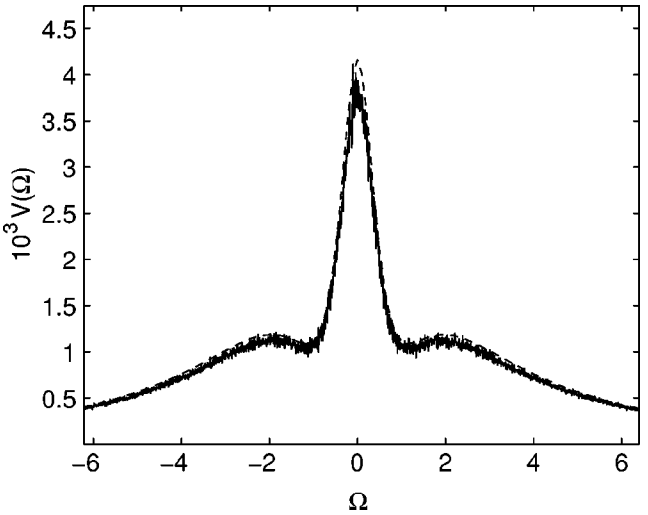

FIG. 8. Nonlinear squeezing spectrum with $g^2=0.001$, $\gamma_r=0.5$, and $\mu=0.9$. The dashed line represents the analytical result and the noisy line the stochastic simulation.

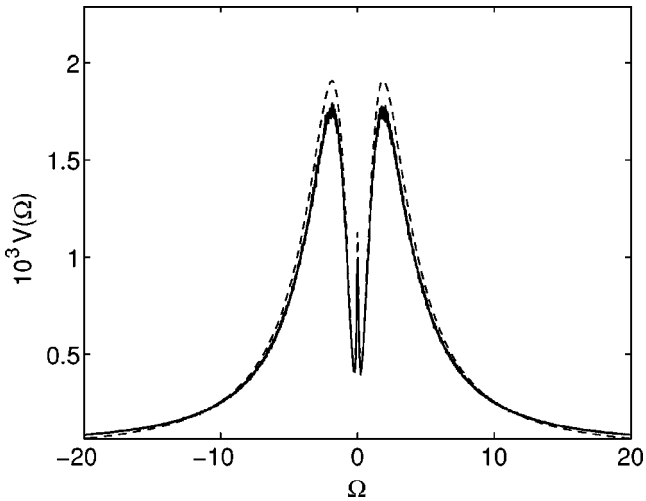

FIG. 9. Nonlinear squeezing spectrum with $g^2=0.001$, $\gamma_r=0.01$, and $\mu=0.93$. The dashed line represents the analytical result and the noisy line the stochastic simulation. This is the driving field for optimum entanglement at zero frequency.

VII. SEMICLASSICAL SPECTRAL CORRELATIONS

In this section we calculate approximate nonlinear results using a semiclassical approach. These are less reliable, especially well below threshold, but have an intuitive "classical" interpretation in terms of the incoming vacuum fluctuations.

A. Wigner representation

In the semiclassical theory, the hierarchy of the stochastic equations given earlier can be written, in the frequency domain, as follows.

First order

$$\tilde{x}_0^{(1)}(\Omega)=\frac{2\gamma_r\xi_{x0}(\Omega)}{(-i\Omega+\gamma_r)},$$

$$\tilde{y}_0^{(1)}(\Omega)=\frac{2\gamma_r\xi_{y0}(\Omega)}{(-i\Omega+\gamma_r)},$$

$$\tilde{x}^{(1)}(\Omega)=\frac{\sqrt{2}\xi_{x1}(\Omega)}{(-i\Omega+1-\mu)},$$

$$\tilde{y}^{(1)}(\Omega)=\frac{\sqrt{2}\xi_{y1}(\Omega)}{(-i\Omega+1+\mu)},$$

$$\tilde{x}^{\dagger(1)}(\Omega)=\frac{\sqrt{2}\xi_{x2}(\Omega)}{(-i\Omega+1-\mu)},$$

$$\tilde{y}^{\dagger(1)}(\Omega)=\frac{\sqrt{2}\xi_{y2}(\Omega)}{(-i\Omega+1+\mu)}. \tag{7.1}$$

Second order

$$\tilde{x}_0^{(2)}(\Omega) = -\frac{\gamma_r[\tilde{x}^{(1)} * \tilde{x}^{\dagger(1)} - \tilde{y}^{(1)} * \tilde{y}^{+(1)}](\Omega)}{(-i\Omega + \gamma_r)},$$

$$\tilde{y}_0^{(2)}(\Omega) = -\frac{\gamma_r[\tilde{x}^{(1)} * \tilde{y}^{+(1)} + \tilde{x}^{\dagger(1)} * \tilde{y}^{(1)}](\Omega)}{(-i\Omega + \gamma_r)},$$

$$\tilde{x}^{(2)}(\Omega) = \frac{[\tilde{x}^{(1)} * \tilde{x}_0^{(1)} + \tilde{y}^{(1)} * \tilde{y}_0^{(1)}](\Omega)}{2(-i\Omega + 1 - \mu)},$$

$$\tilde{y}^{(2)}(\Omega) = \frac{[\tilde{x}^{(1)} * \tilde{y}_0^{(1)} - \tilde{y}^{(1)} * \tilde{x}_0^{(1)}](\Omega)}{2(-i\Omega + 1 + \mu)},$$

$$\tilde{x}^{+(2)}(\Omega) = \frac{[\tilde{x}^{\dagger(1)} * \tilde{x}_0^{(1)} + \tilde{y}^{+(1)} * \tilde{y}_0^{(1)}](\Omega)}{2(-i\Omega + 1 - \mu)},$$

$$\tilde{y}^{+(2)}(\Omega) = \frac{[\tilde{x}^{+(1)} * \tilde{y}_0^{(1)} - \tilde{y}^{+(1)} * \tilde{x}_0^{(1)}](\Omega)}{2(-i\Omega + 1 + \mu)}. \tag{7.2}$$

Third order (signal and idler fields)

$$\tilde{x}^{(3)}(\Omega) = \frac{[\tilde{x}^{(1)} * \tilde{x}_0^{(2)} + \tilde{x}^{(2)} * x_0^{(1)} + \tilde{y}^{(1)} * \tilde{y}_0^{(2)} + \tilde{y}^{(2)} * \tilde{y}_0^{(1)}](\Omega)}{2[-i\Omega + 1 - \mu]},$$

$$\tilde{y}^{(3)}(\Omega) = \frac{[\tilde{x}^{(1)} * \tilde{y}_0^{(2)} + \tilde{x}^{(2)} * \tilde{y}_0^{(1)} - \tilde{y}^{(2)} * \tilde{x}_0^{(1)} - \tilde{y}^{(1)} * \tilde{x}_0^{(2)}](\Omega)}{2[-i\Omega + 1 + \mu]},$$

$$\tilde{x}^{+(3)}(\Omega) = \frac{[\tilde{x}^{+(1)} * \tilde{x}_0^{(2)} + \tilde{x}^{+(2)} * \tilde{x}_0^{(1)} + \tilde{y}^{+(1)} * \tilde{y}_0^{(2)} + \tilde{y}^{+(2)} * y_0^{(1)}](\Omega)}{2[-i\Omega + 1 - \mu]},$$

$$\tilde{y}^{+(3)}(\Omega) = \frac{[\tilde{x}^{+(1)} * \tilde{y}_0^{(2)} + \tilde{x}^{+(2)} * \tilde{y}_0^{(1)} - \tilde{y}^{+(2)} * \tilde{x}_0^{(1)} - \tilde{y}^{+(1)} * \tilde{x}_0^{(2)}](\Omega)}{2[-i\Omega + 1 + \mu]}. \tag{7.3}$$

B. Squeezing correlation spectrum

The spectrum of the squeezed quadrature, for instance, is given by

$$\begin{aligned}\langle \tilde{y}(\Omega_1)\tilde{y}^{+}(\Omega_2)\rangle &= g^2\langle \tilde{y}^{(1)}(\Omega_1)\tilde{y}^{+(1)}(\Omega_2)\rangle \\ &+ g^4\{\langle \tilde{y}^{(2)}(\Omega_1)\tilde{y}^{+(2)}(\Omega_2)\rangle \\ &+ \langle \tilde{y}^{(1)}(\Omega_1)\tilde{y}^{+(3)}(\Omega_2)\rangle + \langle \tilde{y}^{(3)}(\Omega_1)\tilde{y}^{+(1)}(\Omega_2)\rangle\} \\ &+ \ldots . \end{aligned} \tag{7.4}$$

The lowest order contribution turns out to be

$$\langle \tilde{y}^{(1)}(\Omega_1)\tilde{y}^{+(1)}(\Omega_2)\rangle = \frac{2\delta(\Omega_1 + \Omega_2)}{\Omega_1^2 + (1+\mu)^2}. \tag{7.5}$$

Similarly, for the amplified quadrature, to the lowest order we have

$$\langle \tilde{x}^{(1)}(\Omega_1)\tilde{x}^{+(1)}(\Omega_2)\rangle = \frac{2\delta(\Omega_1 + \Omega_2)}{\Omega_1^2 + (1-\mu)^2}. \tag{7.6}$$

For the pump quadratures, there is no squeezing, to the lowest order:

$$\langle \tilde{x}_0^{(1)}(\Omega_1)\tilde{x}_0^{(1)}(\Omega_2)\rangle = \langle \tilde{y}_0^{(1)}(\Omega_1)\tilde{y}_0^{(1)}(\Omega_2)\rangle = \frac{4\gamma_r^2\delta(\Omega_1 + \Omega_2)}{\Omega_1^2 + \gamma_r^2}. \tag{7.7}$$

The next contributions to the squeezed quadrature are

$$\begin{aligned}&\langle \tilde{y}^{(2)}(\Omega_1)\tilde{y}^{+(2)}(\Omega_2)\rangle \\ &= \frac{\gamma_r\delta(\Omega_1 + \Omega_2)}{\Omega_1^2 + (1+\mu)^2}\left\{\frac{1 - \mu + \gamma_r}{(1-\mu)[\Omega_1^2 + (1 - \mu + \gamma_r)^2]}\right. \\ &\left. + \frac{1 + \mu + \gamma_r}{(1+\mu)[\Omega_1^2 + (1 + \mu + \gamma_r)^2]}\right\}\end{aligned} \tag{7.8}$$

and

$$\begin{aligned}&\langle \tilde{y}^{(1)}(\Omega_1)\tilde{y}^{+(3)}(\Omega_2)\rangle + \langle \tilde{y}^{(3)}(\Omega_1)\tilde{y}^{+(1)}(\Omega_2)\rangle \\ &= \frac{2\mu\gamma_r\delta(\Omega_1 + \Omega_2)}{[\Omega_1^2 + (1+\mu)^2]^2} \times \left\{-\frac{(1+\mu)(1 - \mu + \gamma_r) - \Omega_1^2}{(1-\mu)[\Omega_1^2 + (1 - \mu + \gamma_r)^2]}\right. \\ &\left. + \frac{(1+\mu)(1 + \mu + \gamma_r) - \Omega_1^2}{(1+\mu)[\Omega_1^2 + (1 + \mu + \gamma_r)^2]} + \frac{2(1+\mu)}{\gamma_r(1-\mu^2)}\right\},\end{aligned} \tag{7.9}$$

which yield, for the internal spectral correlations,

$$\langle \tilde{Y}(\Omega_1)\tilde{Y}^{+}(\Omega_2)\rangle = \left\{ \frac{2}{\Omega^2+(1+\mu)^2} + \frac{g^2\gamma_r}{[\Omega^2+(1+\mu)^2]^2}\left[\frac{4\mu(1+\mu)}{\gamma_r(1-\mu^2)} + \frac{(1-\mu+\gamma_r)\Omega^2+[(1+\mu)^2+2\mu(1+\mu)](1+\mu+\gamma_r)}{(1+\mu)[\Omega^2+(1+\mu+\gamma_r)^2]} \right.\right.$$
$$\left.\left. + \frac{(1+\mu+\gamma_r)\Omega^2+(1-\mu^2)(1-\mu+\gamma_r)}{(1-\mu)[\Omega^2+(1-\mu+\gamma_r)^2]} \right] + O(g^4) \right\} \delta(\Omega_1+\Omega_2). \tag{7.10}$$

This, in turn, gives the following expression for the external squeezing spectrum, obtained by including both internal fields and the correlated reflected vacuum noise:

$$V^{\pi/2}(\Omega) = 1 - \frac{4\mu}{\Omega^2+(1+\mu)^2} + \frac{2g^2\gamma_r}{[\Omega^2+(1+\mu)^2]^2}\left[\frac{2\mu(1+\Omega^2-\mu^2)}{\gamma_r(1-\mu^2)} \right.$$
$$+ \frac{[(1-\mu)(1-\mu+\gamma_r)-2\mu^2]\Omega^2+(1-\mu+\gamma_r)(1+\mu+\mu^2+\mu^3)}{(1-\mu)[\Omega^2+(1-\mu+\gamma_r)^2]}$$
$$\left. + \frac{[(1+\mu)(1+\mu+\gamma_r)+2\mu^2]\Omega^2+(1+\mu+\gamma_r)(1+3\mu+\mu^2-\mu^3)}{(1+\mu)[\Omega^2+(1+\mu+\gamma_r)^2]} \right] + O(g^4). \tag{7.11}$$

It is interesting to note that this spectrum is quite different from that given by the positive P representation when $\mu \to 0$. However, near the threshold, that is, in the limit $\mu \to 1$, the two results show close agreement. As observed previously in [21], the physical difficulty with the truncated Wigner method is that it is essentially identical with stochastic electrodynamics. This means that even with no input there are changes to the output spectrum caused by the effect of nonlinearities on the vacuum fluctuations, which behave as real classical fields. Just as in the degenerate case, this depends on the damping ratio $\gamma_r = \gamma_0/\gamma$. For $\gamma_r \to 0$, the pump mode has negligible vacuum fluctuation inputs, since $\gamma_0 \approx 0$, so that the truncated Wigner method is more reliable in this limit. Similarly, the approximations used in this method can give nearly correct results at threshold, since here all photon numbers are relatively large.

C. Triple spectral correlation

For the triple spectral correlation function in the truncated Wigner method,

$$\langle \tilde{x}(\Omega_1)\tilde{y}^{+}(\Omega_2)\tilde{y}_0(\Omega_3)\rangle = g^3\langle \tilde{x}^{(1)}(\Omega_1)\tilde{y}^{+(1)}(\Omega_2)\tilde{y}_0^{(1)}(\Omega_3)\rangle$$
$$+ g^4\{\langle \tilde{x}^{(1)}(\Omega_1)\tilde{y}^{+(1)}(\Omega_2)\tilde{y}_0^{(2)}(\Omega_3)\rangle$$
$$+ \langle \tilde{x}^{(2)}(\Omega_1)\tilde{y}^{+(1)}(\Omega_2)\tilde{y}_0^{(1)}(\Omega_3)\rangle$$
$$+ \langle \tilde{x}^{(1)}(\Omega_1)\tilde{y}^{+(2)}(\Omega_2)\tilde{y}_0^{(1)}(\Omega_3)\rangle\} \tag{7.12}$$

The term proportional to g^3 vanishes, and as a result the lowest nontrivial order is found to be

$$\langle \hat{X}(\Omega_1)\hat{Y}^{\dagger}(\Omega_2)\hat{Y}_0(\Omega_3)\rangle$$
$$= \frac{2g\sqrt{\gamma_r}(\gamma_r - i\Omega_3(1+\gamma_r))\,\delta(\Omega_1+\Omega_2+\Omega_3)}{\sqrt{\pi}[\Omega_3^2+\gamma_r^2][\Omega_1^2+(1-\mu)^2][\Omega_2^2+(1+\mu)^2]}. \tag{7.13}$$

This can be compared with the full quantum triple correlations in Eq. (6.19). The essential difference between the quantum and semiclassical theories is that the former gives a zero spectrum in the absence of a driving field while the latter, due to the "real" character of the semiclassical vacuum field, gives a nonzero spectrum. At threshold, the integrated moments in the two methods agree, but even near threshold there are large spectral discrepancies at finite frequencies of $\Omega_3 \simeq \gamma_r/2$, which should be relatively simple to detect due to the large size of the critical fluctuations. This provides a clear distinction between the predictions of a full quantum theory and the truncated Wigner theory (which is equivalent to a semiclassical or hidden variable approach).

VIII. CRITICAL PERTURBATION THEORY

As we have seen, the perturbative corrections diverge at the critical point ($\mu = 1$) and a different approach is called for to investigate the neighborhood of the threshold. To this end we define new scaled quadratures variables, and use a different expansion [38] valid around the critical region. The new pump mode variable x_0 corresponds to the real scaled depletion in the pump mode amplitude, relative to the undepleted value at the critical point. The signal-idler quadrature variables x, x^+ now describe the critical fluctuations scaled to be of order 1 at the threshold.

A. Positive P representation

We scale the quadratures as

$$x_0 = \frac{1}{g}\left[\frac{\chi X_0}{\gamma} - 2 \right], \quad y_0 = \sqrt{\frac{2\gamma_r}{g}}\,Y_0,$$
$$x = \sqrt{g}X, \;\; y = Y,$$
$$x^+ = \sqrt{g}X^+, \;\; y^+ = Y^+, \tag{8.1}$$

and define also a new scaled time and driving field

$$\eta = \frac{2}{g}\left(\frac{\mathcal{E}}{\mathcal{E}_c} - 1 \right),$$

$$\tau = \gamma g t. \tag{8.2}$$

In terms of these variables, the positive P equations become

$$g dx_0 = -\gamma_r[x_0 - 2\eta + x x^+ - g y y^+]d\tau,$$

$$g dy_0 = -\gamma_r[y_0 + x y^+ + y x^+]d\tau,$$

$$dx = \frac{1}{2}(x_0 x + g y_0 y)d\tau + dw_{x1}(\tau),$$

$$g dy = \left[-2y + \frac{g}{2}(x y_0 - y x_0)\right]d\tau + dw_{y1}(\tau),$$

$$dx^+ = \frac{1}{2}(x_0 x^+ + g y_0 y^+)d\tau + dw_{x2}(\tau),$$

$$g dy^+ = \left[-2y^+ + \frac{g}{2}(x^+ y_0 - y^+ x_0)\right]d\tau + dw_{y2}(\tau). \tag{8.3}$$

The Gaussian white noise sources in these equations are no longer uncorrelated and have the following properties:

$$\langle dw_{x1} dw_{x2}\rangle = 2\left(1 + \frac{g}{2}x_0\right)d\tau,$$

$$\langle dw_{y1} dw_{y2}\rangle = -2g\left(1 + \frac{g}{2}x_0\right)d\tau,$$

$$\langle dw_{x1} dw_{y2}\rangle = \langle dw_{x2} dw_{y1}\rangle = g^2 y_0 d\tau. \tag{8.4}$$

We now develop a perturbation theory valid at threshold by expanding in powers of g, as in Eq. (5.6). The first set of equations is obtained by neglecting all terms of order g or greater on the right sides of the two sets of equations given above:

$$g dx_0^{(0)} = -\gamma_r[x_0^{(0)} - 2\eta + x^{(0)} x^{+(0)}]d\tau,$$

$$g dy_0^{(0)} = -\gamma_r[y_0^{(0)} + x^{(0)} y^{+(0)} + y^{(0)} x^{+(0)}]d\tau,$$

$$dx^{(0)} = \frac{1}{2}[x^{(0)} x_0^{(0)}]d\tau + dw_{x1}^{(0)},$$

$$g dy^{(0)} = -2y^{(0)}d\tau + dw_{y1}^{(0)},$$

$$dx^{+(0)} = \frac{1}{2}[x^{+(0)} x_0^{(0)}]d\tau + dw_{x2}^{(0)},$$

$$g dy^{+(0)} = -2y^{+(0)}d\tau + dw_{y2}^{(0)}. \tag{8.5}$$

A significant feature of these equations is that the quadratures $y^{(0)}$ and $y^{+(0)}$ can be worked out without reference to any of other variables, and they give zero noise in the external quadrature at zero frequency. Coupling between variables appears in high order expansions and generates the critical fluctuations in the squeezed quadrature.

We now consider what happens at or near the classical threshold $\eta = 0$. In a model where the subharmonic generation does not cause the pump mode to deplete, we would have $x_0^{(0)} = 2\eta$, and at threshold the critical fluctuations in x and x^+ would diffuse outward without any bound. When depletion is included, the critical fluctuations in these quadratures are finite, but very slowly varying compared to those in the other variables. The pump field can therefore be adiabatically eliminated to first order in the expansion.

Near threshold ($g\eta \ll 1$) the decay term in the unsqueezed quadrature x and x^+ is roughly $-x_0$, which is of order 1. The pump mode will be depleted, so x_0 must be negative in order for this to be stable. The scaled pump field decay is γ_r/g, and the squeezed quadrature decay is of order $1/g$. If γ_r is much larger than g, it is possible to adiabatically eliminate both the pump amplitude and the squeezed quadrature in the equations for the large critical fluctuations x and x^+. Since we are taking the limit of small g, we shall assume that this is possible to zeroth order in the asymptotic expansion. In the adiabatic elimination, we must solve for the steady-state values of the pump x_0, given an instantaneous first order critical fluctuation x and x^+. To leading (zeroth) order this gives

$$x_0^{(0)} = 2\eta - x^{(0)} x^{+(0)}. \tag{8.6}$$

Substituting in the equations for x and x^+, we find that

$$dx^{(0)} = \left[\eta x^{(0)} - \frac{1}{2}(x^{(0)})^2 x^{+(0)}\right]d\tau + dw_{x1}^{(0)},$$

$$dx^{+(0)} = \left[\eta x^{+(0)} - \frac{1}{2}(x^{+(0)})^2 x^{(0)}\right]d\tau + dw_{x2}^{(0)}. \tag{8.7}$$

After the change of variables

$$x_+ = \frac{x^{(0)} + x^{+(0)}}{2} \quad x_- = i\frac{x^{(0)} - x^{+(0)}}{2}. \tag{8.8}$$

Equation (8.7) can be put in the form

$$\dot{\mathbf{x}} = -\eta\mathbf{x} - \frac{1}{2}\mathbf{x}(\mathbf{x}\cdot\mathbf{x}) + \xi(t), \tag{8.9}$$

where $\mathbf{x}$ is a two-component vector whose elements are x_+ and x_-.

It is possible to write the Fokker-Planck equation for the probability density $P(x_+, x_-, t)$, and look for the equilibrium distribution of the form $P(\mathbf{x}) = N\exp[-U(\mathbf{x})]$, where $U(\mathbf{x})$ is a potential function given by

$$U(\mathbf{x}) = \eta\mathbf{x}\cdot\mathbf{x} + \frac{1}{4}(\mathbf{x}\cdot\mathbf{x})^2. \tag{8.10}$$

The variance of the critical fluctuations at the critical point $\eta = 0$ is given by

$$\langle \hat{X}\hat{X}^\dagger\rangle = \frac{2}{g\sqrt{\pi}} = \frac{1.128\ldots}{g}. \tag{8.11}$$

By comparison, the corresponding intracavity critical fluctuation variance in a degenerate OPO at a comparable input flux [21,38] is

$$\langle \hat{X}_{DG}^2\rangle = \frac{2\sqrt{2}\Gamma(3/4)}{g\Gamma(1/4)} = \frac{0.956\ldots}{g}. \tag{8.12}$$

B. Critical squeezing in positive *P* representation

We can now find the steady-state variance of the squeezed quadrature at threshold. Because the fluctuations in the squeezed quadrature are very small, we must work to higher order in the asymptotic expansion to obtain a nontrivial result. To achieve this, it is most useful to introduce equations in the higher order moments yy^+ and $z=x^+y+xy^+$. The corresponding stochastic equations are derived using Itô rules for the variable changes, so that

$$gd(yy^+) = -2\left[1 + 2yy^+ + \frac{g}{2}\left(x_0 + x_0 yy^+ - \frac{1}{2}y_0 z\right)\right]d\tau + y dw_{y2} + y^+ dw_{y1},$$

$$gdz = \left[-2z + \frac{g}{2}y_0(2xx^+ + 2gyy^+ + 4g)\right]d\tau + x dw_{y2} + x^+ dw_{y1} + gy dw_{x2} + gy^+ dw_{x1}. \tag{8.13}$$

Taking the expectation value at the steady state $\langle d(yy^+)\rangle = 0$, we get the first order correction

$$\langle yy^+\rangle^{(1)} = -\frac{g}{4}\left\langle (1 + yy^+)x_0 - \frac{1}{2}y_0 z\right\rangle^{(0)}. \tag{8.14}$$

The first term in the above expression gives the result

$$\langle (1 + yy^+)x_0\rangle^{(0)} = \frac{1}{2}\langle x_0\rangle^{(0)} = \eta - \frac{1}{2}\langle x^{(0)}x^{+(0)}\rangle. \tag{8.15}$$

For the second term we must write the correlation from the following equation:

$$gd(y_0 z) = -[(2 + \gamma_r)y_0 z + \gamma_r z^2]d\tau + 0(g) + (\text{noise}), \tag{8.16}$$

and then we get

$$\langle y_0 z\rangle^{(0)} = -\frac{\gamma_r}{2 + \gamma_r}\langle z^2\rangle^{(0)} = -\frac{\gamma_r}{2 + \gamma_r}\langle (x^+y + xy^+)^2\rangle^{(0)} = \frac{\gamma_r}{2 + \gamma_r}\langle x^{(0)}x^{+(0)}\rangle. \tag{8.17}$$

Finally we obtain, to first order,

$$\langle \hat{Y}\hat{Y}^\dagger\rangle = \frac{1}{2} - \frac{g}{4}\left(\eta - \frac{1}{2}\langle x^{(0)}x^{+(0)}\rangle\right) + \frac{g}{8}\left(\frac{\gamma_r}{2 + \gamma_r}\right)\langle x^{(0)}x^{+(0)}\rangle = \frac{1}{2} - \frac{g\eta}{4} + \frac{g^2}{8}\left(\frac{2 + 2\gamma_r}{2 + \gamma_r}\right)\langle \hat{X}\hat{X}^\dagger\rangle. \tag{8.18}$$

Noting that $\langle \hat{X}\hat{X}^\dagger\rangle$ is given by Eq. (8.11), this result shows that the best squeezing, in the *overall* moment, for the intracavity combined mode quadrature occurs just above threshold where the last two terms nearly cancel. In the degenerate OPO [21] the corresponding moment is given by

$$\langle \hat{Y}^2_{DG}\rangle = \frac{1}{2} - \frac{g\eta}{2\sqrt{2}} + \frac{g^2}{8\sqrt{2}}\left(\frac{2 + 3\gamma_r}{2 + \gamma_r}\right)\langle \hat{X}^2_{DG}\rangle. \tag{8.19}$$

It should be recalled here that in this case the value of $\langle X^2_{DG}\rangle$ is given by Eq. (8.12). We can interpret this result physically by recalling that as one passes the critical point the nondegenerate parametric amplifier develops a completely different type of squeezing [12] from the below-threshold case. Instead of quadrature squeezing, there is a phase-number squeezing which develops above threshold. This involves correlations which may be thought of as occupying a curved region in the conventional X, Y phase space. Thus, the below-threshold correlations are destroyed by phase curvature as well as by the obvious saturation effects that are found in the degenerate case.

C. Wigner representation

As in the positive *P* equations, we define new scaled quadrature variables to avoid divergences at the critical point:

$$x_0 = \frac{1}{g}\left[\frac{\chi X_0}{\gamma} - 2\right],\quad \gamma_0 = \sqrt{2\gamma_r}Y_0,$$

$$x = \sqrt{g}X,\ y = Y,$$

$$x^+ = \sqrt{g}X^+,\ y^+ = Y^+. \tag{8.20}$$

In these new variables, the stochastic equations in the Wigner representation are

$$gdx_0 = -\gamma_r[x_0 - 2\eta + xx^+ - gyy^+]d\tau + dw_{x0}(\tau),$$

$$gdy_0 = -\gamma_r[\gamma_0 + \sqrt{g}(xy^+ + yx^+)]d\tau + dw_{y0}(\tau),$$

$$dx = \frac{1}{2}(x_0 x + \sqrt{g}y_0 y)d\tau + dw_{x1}(\tau),$$

$$gdy = \left[-2y + \frac{1}{2}(\sqrt{g}xy_0 - gyx_0)\right]d\tau + dw_{y1}(\tau),$$

$$dx^+ = \frac{1}{2}(x_0 x^+ + \sqrt{g}y_0 y^+)d\tau + dw_{x2}(\tau),$$

$$gdy^+ = \left[-2y^+ + \frac{1}{2}(\sqrt{g}x^+\gamma_0 - gy^+x_0)\right]d\tau + dw_{y2}(\tau). \tag{8.21}$$

Here we use the same notation for scaled time and driving field as in the positive *P* case. The noise correlations are given by

$$\langle dw_{x0}dw_{y0}\rangle = 4\gamma_r^2 g d\tau,$$

$$\langle dw_{x1}dw_{x2}\rangle = 2d\tau,$$

$$\langle dw_{y1}dw_{y2}\rangle = 2g d\tau. \tag{8.22}$$

To develop a perturbation scheme, we define the zero-order approximation to be the one in which terms of order and greater than $\sqrt{g}$ are neglected in the set of equations above:

$$gdx_0^{(0)} = -\gamma_r[x_0^{(0)} - 2\eta + x^{(0)}x^{+(0)}]d\tau + dw_{x0}^{(0)},$$

$$gdy_0^{(0)} = -\gamma_r[\gamma_0^{(0)} + x^{(0)}y^{+(0)} + y^{(0)}x^{+(0)}]d\tau + dw_{y0}^{(0)},$$

$$dx^{(0)} = \frac{1}{2}[x^{(0)}x_0^{(0)}]d\tau + dw_{x1}^{(0)},$$

$$gdy^{(0)} = -2y^{(0)}d\tau + dw_{y1}^{(0)},$$

$$dx^{+(0)} = \frac{1}{2}[x^{+(0)}x_0^{(0)}]d\tau + dw_{x2}^{(0)},$$

$$gdy^{+} = -2y^{+(0)}d\tau + dw_{y2}^{(0)}. \tag{8.23}$$

It is worth noting that this set of equations, though having the same structure as that in the positive P case, has differences in the correlations of the noise terms. On adiabatic elimination of the pump and substituting this result into x^0 and x^{+0} we find the same equations as in the positive P representation, since to zeroth order the correlation noise in both theories is identical.

D. Critical squeezing in Wigner representation

Now we proceed to calculate $\langle yy^+\rangle$ at threshold using the Wigner representation. Using the Itô rules we get

$$gd(yy^+)2 - 4yy^+ + \frac{\sqrt{8}}{2}y_0 z - \frac{g}{2}2yy^+x_0 + dw_{y1} + dw_{y2}, \tag{8.24}$$

where we have defined $z = yx^+ + y^+x$, which obeys the following equation:

$$gdz = -2z + \sqrt{g}y_0 xx^+ + g\sqrt{g}y_0 yy^+ + x^+dw_{y1} + gydw_{x2} + xdw_{y2} + gy^+dw_{x1}. \tag{8.25}$$

The squeezing variance at threshold in the steady state is obtained from the above equation taking expectation values

$$\langle yy^+\rangle = \frac{1}{2} + \frac{\sqrt{g}}{8}\langle y_0 z\rangle - \frac{g}{4}\langle x_0 yy^+\rangle. \tag{8.26}$$

The last term of the above equation can be written as

$$\frac{g}{4}\langle x_0^{(0)}\rangle\langle yy^+\rangle^{(0)} = \frac{g\eta}{4} - \frac{g}{8}\langle x^{(0)}x^{+(0)}\rangle, \tag{8.27}$$

and Eq. (8.24) gives the result

$$\langle y_0 z\rangle^{(0)} = -\sqrt{g}\frac{\gamma_r\langle z^2\rangle^{(0)}}{2+\gamma_r} + \sqrt{g}\frac{\langle y_0^2\rangle^{(0)}\langle x^{(0)}x^{+(0)}\rangle}{2+\gamma_r}. \tag{8.28}$$

Using the results derived from the zero-order equations

$$\langle y_0^2\rangle^{(0)} = 2\gamma_r,$$

$$\langle z^2\rangle^{(0)} = 2\langle x^{(0)}x^{+(0)}\rangle\langle y^{(0)}y^{+(0)}\rangle, \tag{8.29}$$

we finally obtain

$$\langle \hat{Y}\hat{Y}^\dagger\rangle = \frac{1}{2} - \frac{g\eta}{4} + \frac{g}{8}\left(\frac{2+2\gamma_r}{2+\gamma_r}\right)\langle \hat{X}\hat{X}^\dagger\rangle. \tag{8.30}$$

This result is exactly the same as we obtained using the positive P representation. We can infer that dropping third order terms in the Wigner phase space equation does not have any direct consequence for the near-threshold analysis of bipartite entanglement to this order of approximation. This is to be contrasted with the situation far below threshold, where there are large differences in the nonlinear contributions, indicating a failure of the truncated (hidden variable) Wigner theory.

The change in behavior has a simple mathematical origin. Far below threshold, the signal and idler photon numbers are small, which leads to a failure of the truncation approximation when using the semiclassical method. At the critical point, photon numbers in all modes are relatively large, so the truncation approximation has less severe consequences.

IX. CONCLUSIONS

We have calculated the effects of nonlinear quantum fluctuations in a nondegenerate parametric oscillator, both below and at the classical threshold, using stochastic equations that follow from the positive P representation, as well as using truncated Wigner methods.

The analytical results thus obtained are compared with exact numerical simulations. The spectral entanglement and squeezing in the output fields are maximized just below threshold. This may be useful, for example, in cryptographic applications [39]. We find that at the critical point ($\mu=1$), the scaling behavior is quite different from the behavior below threshold, and must be calculated by using an asymptotic perturbation theory, valid at the threshold itself. The total intracavity squeezing and entanglement moment is actually minimized at a driving field just above threshold. This apparent paradox can be attributed to the fact that the critical fluctuations mostly tend to broaden the squeezing spectrum, which has a strong effect at zero frequency but does not diminish the total squeezing moment, integrated over all frequencies.

A similar analysis was carried out within the framework of the semiclassical theory arising from a truncation to a Fokker-Planck form of the evolution equation in the Wigner representation. Here, we found that well below threshold, while the linear terms agreed with the full quantum calculation, the nonlinear corrections tend to disagree, especially for low subharmonic losses. However, at the critical point, the situation changes. Here, where the dominant terms are nonlinear, we find excellent agreement between the two methods. While quantum fluctuations are indeed large at the critical point, it appears that an equally acceptable interpretation of the observed noise characteristics near the critical point exists via a semiclassical model, which is essentially a kind of hidden variable theory.

We have also compared these results with those obtained by using two degenerate parametric oscillators together with a beam splitter. While this method creates similar entanglement far below threshold, it is not identical at or near thresh-

old. In this region, where nonlinearities become important, the approach of having two degenerate oscillators is quite different from the nondegenerate case. We find that under comparable total input photon flux conditions the degenerate method is generally less efficient at creating an entangled output. This is due to the fact that, as two pump beams are needed, a larger nonlinearity is required for comparable entanglement in the output, when the total power input is matched with the nondegenerate case. This leads to larger nonlinear corrections near threshold. These differences vanish in the limit of a low loss pump mode. However, in practice there are other losses as well as those caused by the input and output couplers, which could lead to different efficiencies as well.

Our main result is that entanglement, EPR correlations, and squeezing are optimized very near threshold. In this region, the semiclassical Wigner approximation can give an excellent description of the squeezing and entanglement fluctuations, although it is unable to correctly predict the nonlinear corrections far below threshold. On the other hand, some highly nonclassical signatures of quantum effects occur in the tripartite correlations, which are not described correctly by the semiclassical, hidden variable approach. Surprisingly, these nonclassical and non-Gaussian signatures persist well below threshold, where one might have expected the usual linearized analysis to be applicable. Large discrepancies in the third order spectral correlations are also found even very close to threshold, where the relevant fluctuations are large.

This suggests that experimental tests of the present theory may be carried out near threshold—where large effects are predicted in the enhanced critical fluctuations of the unsqueezed quadrature and in the nonclassical triple spectral correlations.

ACKNOWLEDGMENTS

We gratefully acknowledge financial support from CNPq (Brazil) and the Australian Research Council Centre of Excellence program.

[1] A. Yariv, *Quantum Electronics* (Wiley, New York, 1989).
[2] L. A. Wu, H. J. Kimble, J. L. Hall, and H. Wu, Phys. Rev. Lett. **57**, 2520 (1986).
[3] A. Heidmann, R. J. Horowicz, S. Reynaud, E. Giacobino, C. Fabre, and G. Camy, Phys. Rev. Lett. **59**, 2555 (1987).
[4] C. K. Hong, Z. Y. Ou, and L. Mandel, Phys. Rev. Lett. **59**, 2044 (1987).
[5] Z. Y. Ou, S. F. Pereira, H. J. Kimble, and K. C. Peng, Phys. Rev. Lett. **68**, 3663 (1992).
[6] Yun Zhang, Hai Wang, Xiaoying Li, Jietai Jing, Changde Xie, and Kunchi Peng, Phys. Rev. A **62**, 023813 (2000).
[7] W. P. Bowen, R. Schnabel, P. K. Lam, and T. C. Ralph, Phys. Rev. Lett. **90**, 043601 (2003).
[8] Ch. Silberhorn, P. K. Lam, O. Weiss, F. Konig, N. Korolkova, and G. Leuchs, Phys. Rev. Lett. **86**, 4267 (2001).
[9] A. Einstein, B. Podolsky, and N. Rosen, Phys. Rev. **47**, 777 (1935).
[10] M. D. Reid and P. D. Drummond, Phys. Rev. Lett. **60**, 2731 (1988); P. Grangier, M. J. Potasek, and B. Yurke, Phys. Rev. A **38**, 3132 (1988); B. J. Oliver and C. R. Stroud, Phys. Lett. A **135**, 407 (1989).
[11] M. D. Reid, Phys. Rev. A **40**, 913 (1989); e-print quant-ph/0112038.
[12] M. D. Reid and P. D. Drummond, Phys. Rev. A **40**, 4493 (1989);P. D. Drummond and M. D. Reid, *ibid.* **41**, 3930 (1990).
[13] S. Feng and O. Pfister, J. Opt. B: Quantum Semiclassical Opt. **5**, 262 (2003); e-print quant-ph/0310002.
[14] L. M. Duan, G. Giedke, J. I. Cirac, and P. Zoller, Phys. Rev. Lett. **84**, 2722 (2000); R. Simon, *ibid.* **84**, 2726 (2000).
[15] N. Korolkova *et al.*, Eur. Phys. J. D **18**, 229 (2002).
[16] C. Schori, J. L. Sorensen, and E. S. Polzik, Phys. Rev. A **66**, 033802 (2002).
[17] T. W. Marshall and E. Santos, Phys. Rev. A **41**, 1582 (1990).
[18] K. Dechoum, T. W. Marshall, and E. Santos, J. Mod. Opt. **47**, 1273 (2000).
[19] M. K. Olsen, S. C. G. Granja, and R. J. Horowicz, Opt. Commun. **165**, 293 (1999).
[20] M. K. Olsen, K. Dechoum, and L. I. Plimak, Opt. Commun. **190**, 261 (2001).
[21] S. Chaturvedi, K. Dechoum, and P. D. Drummond, Phys. Rev. A **65**, 033805 (2002); P. D. Drummond, K. Dechoum, and S. Chaturvedi, *ibid.* **65**, 033806 (2002).
[22] *Quantum Squeezing*, edited by P. D. Drummond and Z. Ficek (Springer, Berlin, 2003).
[23] R. Graham and H. Haken, Z. Phys. **210**, 276 (1968); R. Graham, *ibid.* **210**, 319 (1968); **211**, 469 (1968).
[24] K. J. McNeil and C. W. Gardiner, Phys. Rev. A **28**, 1560 (1983).
[25] H. J. Carmichael, *Statistical Methods in Quantum Optics 1* (Springer, Berlin, 1999).
[26] S. Chaturvedi, P. D. Drummond, and D. F. Walls, J. Phys. A **10**, L187 (1977); P. D. Drummond and C. W. Gardiner, *ibid.* **13**, 2353 (1980).
[27] A. Gilchrist, C. W. Gardiner, and P. D. Drummond, Phys. Rev. A **55**, 3014 (1997).
[28] L. Arnold, *Stochastic Differential Equations: Theory and Applications*, (John Wiley and Sons, New York, 1974);C. W. Gardiner, *Handbook of Stochastic Methods* (Springer, Berlin, 1983).
[29] H. J. Carmichael, *An Open Systems Approach to Quantum Optics* (Springer, New York, 1993).
[30] P. Deuar and P. D. Drummond, Phys. Rev. A **66**, 033812 (2002).
[31] C. J. Mertens, T. A. B. Kennedy, and S. Swain, Phys. Rev. A **48**, 2374 (1993); L. I. Plimak and D. F. Walls, *ibid.* **50**, 2627 (1994); C. J. Mertens and T. A. B. Kennedy, *ibid.* **53**, 3497 (1996).
[32] B. Yurke, Phys. Rev. A **32**, 300 (1985).
[33] C. W. Gardiner and M. J. Collett, Phys. Rev. A **31**, 3761

(1985); M. J. Collett and D. F. Walls, *ibid.* **32**, 2887 (1985).
[34] A. Furusawa, J. L. Sorenson, S. L. Braunstein, C. A. Fuchs, H. J. Kimble, and E. S. Polzik, Science **282**, 706 (1998).
[35] C. M. Caves and B. L. Schumaker, Phys. Rev. A **31**, 3068 (1985); B. L. Schumaker and C. M. Caves, *ibid.* **31**, 3093 (1985).
[36] S. Chaturvedi and P. D. Drummond, Eur. Phys. J. B **8**, 251 (1999).
[37] P. D. Drummond and P. Kinsler, J. Eur. Opt. Soc. B **7**, 727 (1995); S. Chaturvedi and P. D. Drummond, Phys. Rev. A **55**, 912 (1997).
[38] P. Kinsler and P. D. Drummond, Phys. Rev. A **52**, 783 (1995).
[39] T. C. Ralph, Phys. Rev. A **61**, 010303 (1999); **62**, 062306 (2000); M. Hillery, *ibid.* **61**, 022309 (1999); M. D. Reid, *ibid.* **62**, 062308 (2000); N. J. Cerf, M. Levy, and G. Van Assche, *ibid.* **63**, 052311 (2001); S. F. Pereira, Z. Y. Ou, and H. J. Kimble, *ibid.* **62**, 042311 (2000); P. Navez, E. Brambilla, A. Gatti, and L. A. Lugiato, *ibid.* **65**, 013813 (2002); C. Silberhorn, T. C. Ralph, N. Lutkenhaus, and G. Leuchs, Phys. Rev. Lett. **89**, 167901 (2002);C. Silberhorn, N. Korolkova, and G. Leuchs, *ibid.* **88**, 167902 (2002); F. Grosshans and P. Grangier, *ibid.* **88**, 057902 (2002).